

Continuous Flow Hydrothermal Synthesis of ZSM-5 Zeolite

by

Jiayuan Li

Bachelor of Science, University of Massachusetts, 2020

Submitted to the Graduate Faculty of the
Swanson School of Engineering in partial fulfillment
of the requirements for the degree of
Master of Science in Chemical Engineering

University of Pittsburgh

2022

UNIVERSITY OF PITTSBURGH

SWANSON SCHOOL OF ENGINEERING

This thesis was presented

by

Jiayuan Li

It was defended on

March 30, 2022

and approved by

Lei Li, Ph.D., Associate Professor, Department of Chemical and Petroleum Engineering

James R. McKone, Ph.D., Assistant Professor, Department of Chemical and Petroleum
Engineering

Thesis Advisor: Götz Vesper, Ph.D., Professor, Department of Chemical and Petroleum
Engineering

Copyright © by Jiayuan Li

2022

Continuous Flow Hydrothermal Synthesis of ZSM-5 Zeolite

Jiayuan Li, M.S.

University of Pittsburgh, 2022

ZSM-5 is a particularly important zeolite to the industry owing to its unique structure and exceptional properties. It is typically synthesized under hydrothermal conditions in batch reactors. The batch synthesis method involves heating the reactants in an autoclave that is continually operated at high temperatures and autogenous pressures for several hours or even a few days to finish the synthesis, which is highly wasteful in terms of energy, time, and operation. In light of the vast demands for zeolites and their wide range of applications, developing a fast and efficient synthesis process is highly desirable. Herein, we present a continuous flow synthesis process for ZSM-5 with vastly accelerated synthesis times (seconds rather than days) and a high production rate (~ 590 g/day). The approach is based on the direct mixing of a zeolite precursor with hot pressurized water in a tubular flow reactor, resulting in a rapidly achieved high-temperature condition (~280 °C, 100 bar) to accelerate zeolite crystallization, followed by rapid cooling to prevent undesired reactions. By combining the excellent mass transfer rate in a continuous flow reactor with the instantaneous heating achieved by the direct mixing with pressurized hot water, this design can facilitate the future mass production of zeolites.

Table of Contents

Preface.....	xiii
1.0 Introduction.....	1
1.1 Background Information.....	1
1.1.1 Zeolites	1
1.1.2 ZSM-5 Zeolite.....	3
1.1.3 Hydrothermal Synthesis of ZSM-5 – Reagents, Nucleation/Growth, and Mechanisms	6
1.1.3.1 Synthesis and Reagents	6
1.1.3.2 Nucleation and Growth.....	9
1.1.3.3 Mechanism.....	10
1.1.4 Transition from Batch Hydrothermal to Continuous Flow Hydrothermal Synthesis.....	12
1.1.5 Continuous Flow Hydrothermal Synthesis of Zeolites – Opportunities and Challenges.....	15
1.2 Project Objectives.....	21
1.3 Outline of the Thesis.....	21
2.0 Materials and Methods.....	23
2.1 Materials.....	23
2.2 Preparation of Synthesis Mixture for ZSM-5.....	23
2.3 Batch Hydrothermal synthesis	24
2.4 Design and Setup	24

2.5 Continuous Synthesis	26
2.6 Computational Fluid Dynamics Modelling	27
2.7 Zeolite Characterization	28
2.7.1 X-ray Powder Diffraction and Relative Crystallinity	28
2.7.2 Electron Microscopy	29
2.7.3 Surface Area	29
2.7.4 Yield.....	29
3.0 Results and Discussions	30
3.1 Mixing Efficiency in Different Configurations	30
3.2 Undesired Preheating of the Precursor gel	33
3.3 Effect of Reactor Fouling on Conversion	35
3.4 Heat Loss and Temperature Control.....	39
3.5 Effect of Reaction Temperature on Conversion	42
3.6 Effect of Residence time on Crystallinity and Particle Size	46
3.7 Continuous vs Batch Synthesis – Yield and Production Rate	51
4.0 Conclusions and Outlook.....	56
4.1 Conclusion	56
4.2 Outlook	57
Appendix A Supplemental Materials	60
Bibliography	63

List of Tables

Table 1. Weight of samples collected from different sources.....	54
---	-----------

List of Figures

Figure 1. Tens of unique zeolite structures all emerge from the simple tetrahedron from ref.[1].	2
Figure 2. Skeleton diagram of ZSM-5 (a) pentasil unit (b) linkage of pentails units from ref.[7].	3
Figure 3. (a) Perpendicular and regular channels in ZSM-5 lattice, the intersections become cages. (b) ZSM-5 sheet (010) from ref.[7], (c) (100) from ref.[7].	4
Figure 4. Bronsted acid sites in ZSM-5 lattice from ref.[5].	5
Figure 5. An illustration of general procedures for hydrothermal synthesis in an autoclave from ref.[17].	7
Figure 6. The famous LaMer model of nucleation and growth from ref.[30].	10
Figure 7. Growth Mechanism of ZSM-5 in the presence of TPA proposed by Burkett (during his PH. D study) and Davis in 1994 from ref. [34].	11
Figure 8. A general schematic for CFHS process.	14
Figure 9. (a) World’s largest multi-nanomaterial Promethean Particles 1000 tons NPs per year 2016. (b) The world’s first commercial CFHS facility for a large-scale production of LiFePO₄ (Hanwha Chemical Corporation). 2011.	15
Figure 10: A schematic showing designs of different reactor components in CFHS process. (a) A ‘fouling-free’ focusing flow reactor where the reactor wall is shielded against the reagents stream by the ‘sheath flow. The diffusion flow prevents the precursor from the core from meeting the ‘sheath’ flow at walls [61]. (b) Countercurrent mixer designed by Lester Group [62, 63]. (c) Computational fluid dynamics	

simulation result of a swirling tee showing a turbulent mixing regime[65]. (d) Segmented flow setup where the precursor is dispersed in oil to form an emulsion phase and then mixed with the hot water into the reactor [66]. (e) A pressure chamber acts as a BPR where product slurry is collected in the chamber. The chamber has a maximum 1L capacity and can safely handle temperatures up to 140 °C and 10 bar of pressure [67]...... 20

Figure 11. A detailed schematic showing the full continuous synthesis setup..... 24

Figure 12. A demonstration of the 3D tee-mixer (1/4'') built in COMSOL Multiphysics... 28

Figure 13. Temperature profile of the mixing between precursor at 4 ml/min, 25 °C, and hot water at 16 ml/min, 300 °C in a 1/4'' T mixer in different configurations (a): injecting precursor from the bottom, (b) injecting hot water from the bottom, (c) symmetrical mixing of precursor and hot water. Radial temperature distributions are shown every 0.244 mm downstream of the mixing point in (b) and (c)..... 32

Figure 14. COMSOL simulation results of mixing water at 1 ml/min, 280 °C and precursor at 0.8 ml/min, 90 °C in a 1/4'' T mixer in steady state. (a) Temperature gradient plot at the outer wall and fluid surface using stainless steel pipe in the gel feed line. (b) using ceramic pipe in the gel feed line, (c) comparison of precursor temperature when flowing towards the mixing point. 34

Figure 15. A photo showing the fouling observed in a 1/2'' tubular reactor after a synthesis at ~280 C for 20 mins..... 36

Figure 16. Characterization results of products obtained from continuous flow synthesis in a 1/8'' tubular reactor at different temperatures in 12 s. (a) A photo showing the blocked tubular reactor after a synthesis carried out at 240 C. (b) XRD patterns of

the samples obtained at 200 C and 150 C. (c) SEM image of the sample obtained at 150 C, (d) SEM image of the sampled obtained at 200 C..... 37

Figure 17. Characterization results of products obtained from continuous flow synthesis in a 1/4” tubular reactor at different temperatures in 45 s (a) XRD patterns of the samples obtained at 223 C and 230 C and 244 C (b) SEM image of the sample obtained at 223 C, (c) SEM image of the sampled obtained at 244 C..... 38

Figure 18. Temperatures in the system measured when mixing precursor at 4 ml/min, 25 °C with water at different flow rates. The temperature of water decreases as the flow rate increases due to insufficient heating. TR1 is the temperature measured right after the mixing union, and TR2 is the temperature measured at reactor exit (see Fig.S2 b). Temperature drop is the difference between TR1 and TR2..... 40

Figure 19. XRD patterns of products obtained in continuous flow synthesis in a 1/2 ‘tubular reactor at different temperatures in 45 s. The feed conditions were precursor at 4 ml/min, 25 C, water at 16 ml/min..... 42

Figure 20. SEM images of samples obtained from the continuous flow reactor 1/2” (a) at 249 °C, 45 s, (b) 266 °C, 45s, (c) 282 °C, 45s, at different magnifications (left) 5 k and (right) 25 k. 45

Figure 21. (a) XRD patterns of products obtained in continuous flow synthesis in a 1/2 ‘ tubular reactor at ~ 280 °C in different residence times. The feed conditions were precursor at 4 ml/min, 25 C, water at 16 ml/min. (b) Zoomed-in XRD patterns of the products between 22-25. (c) Relative crystallinity of the products obtained in the different residence times as well as the silicon to aluminum ratio and the BET surface area of the 75 s and batch synthesized samples. 48

Figure 22. SEM images of the samples obtained from the continuous flow reactor ½' ' (a) at 282 °C, 45 s, (b) 276 °C, 60s, (c) 276 °C, 75 s, (d) batch synthesis at 170 °C, 24 hr., at different magnifications (left) 5 k and (right) 25 k..... 50

Figure 23. (a) Pressure profile and (b) temperature profile during continuous synthesis in a ½'' reactor at 276 C, 75s..... 52

Figure 24. SEM images (left) and particle size distributions (right) of samples collected (a) at the outlet, (b) from solids flushed out of the filters (c) from the solids stuck in the filters, (d) residual particles cleaned out of the system..... 53

Figure 25: Photos showing (a) reactor fouling, (b) particle deposition in the filter, (c) particles settled to the bottom of tubing 54

Figure S 1. Detailed illustration of the continuous flow apparatus used for the ultrafast synthesis of zeolites. Please see Fig 27 to Fig 29 for zoomed in views of specific sections. 60

Figure S 2. Photo showing (a) reactor ready for running synthesis, (b) the reactor after removing the insulations and the vibrator. The reactor length is defined as the distance from the midpoint in the T mixer to the end of the tubular reactor as shown in the picture..... 60

Figure S 3. Detailed illustration of the parallel filter setup. When Filter 1 is blocked, 3V-1 and 3V-2 are switched to Filter 2 to allow a continuous flow of product stream (Red Line) while Filter 1 is being flushed with water (Green line). 61

Figure S 4. Photo showing (a) the connection of vibrator to system tubing, (b) PTFE-lined tube in precursor feed line. 61

Figure S 5. Peak deconvolution on XRD patterns of (a) batch synthesized ZSM-5, (b) product obtained at 276 °C, 75s in continuous synthesis. The position (2-theta) and height (intensity) of the deconvoluted peaks are shown on the top of each individual peak. It can be observed that the peaks centered at 23.15° in the sample in continuous synthesis are broadened and the ratio of the doublets is smaller 62

Figure S 6. Samples collected from a typical continuous flow synthesis after 20 mins. (a) Aqueous slurry flushed out of the filters, (b) deposited particles retrieved from the filters, (c) aqueous slurry collected and the outlet, (d) residue cleaned out of the system. 62

Preface

I would like to give my earnest thanks to my advisor Dr. Vesper for mentoring me. Without his dedicated support and guidance, this work would not have been possible.

I would like to acknowledge and thank my coworker Runze Zhao for his contribution to this work. Working with you has been a great pleasure for me.

I am also grateful to Yifan Deng for providing advice and doing most of the material characterizations in this work.

Lastly, I would like to thank my family, friends and everyone who has helped me along my way.

1.0 Introduction

1.1 Background Information

1.1.1 Zeolites

Zeolites are crystalline, microporous materials featuring regular openings (often called pores or cavities) interconnected through narrow channels in highly ordered arrays. Zeolites are often referred to as 'molecular sieves', because the pores and channels (ca. 3-15 Å) in zeolite frameworks have uniform sizes and are similar to small molecules such as cations, water, or suitable-sized molecules. Zeolites are aluminosilicates, and their frameworks are based on tetrahedral silica (SiO_4) and tetrahedral aluminum (AlO_4^-), as shown in Fig.1. The tetrahedrons are linked at their corners via shared oxygen atoms, extending into a three-dimensional network with different structures. Due to the charge imbalance arising from the difference in valency between Al and Si and the number of AlO_4^- and SiO_4 present in the framework, protons, alkalis, or alkaline earth metals are filled into the lattice to balance the charge.

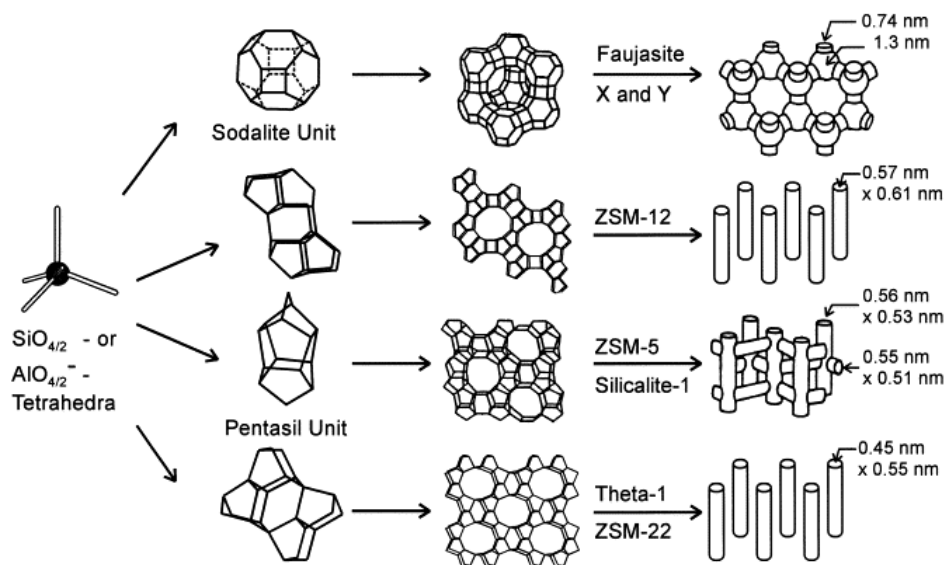


Figure 1. Tens of unique zeolite structures all emerge from the simple tetrahedron from ref.[1].

Zeolites occur in nature where volcanic ashes react with alkaline groundwater. So far, 40 natural zeolites have been discovered. Natural zeolites have found many applications, such as being adsorbents for heavy metals in wastewater treatment and being carriers for agricultural compounds in the treatment of soil and fishponds [2]. However, natural zeolites have limited applications in the industries due to impurity phases and inconsistency in compositions in the frameworks. In the late 1940s, Richard Barrer discovered the first synthetic zeolite [3]. Then, Robert Milton pioneered in using a variety of starting materials to synthesize 20 different zeolites by 1953 [4]. Until today, 191 synthetic zeolites have been made [3]. In fact, most of the zeolites used in the industry today are synthetic zeolites that are tuned in structures and compositions for desired properties regarding different applications, such as catalysis, ion exchange, and separations [5]. With continuously increasing demands for zeolites with specific chemical and physical properties, research on novel zeolites and synthesis routes remains to be a vital field in the future.

1.1.2 ZSM-5 Zeolite

ZSM-5 (Zeolite Socony Mobile-5) is an important zeolite that represents the family of pentasil and “high silica” zeolite ($\text{Si}/\text{Al} > 10$). It was invented and patented by R. J. Argauer and G. R. Landolt (Socony Mobile) in 1972 [6].

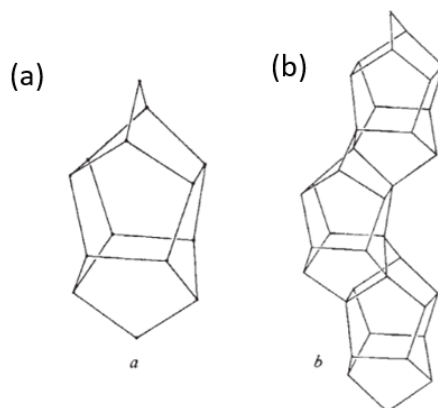


Figure 2. Skeleton diagram of ZSM-5 (a) pentasil unit (b) linkage of pentails units from ref.[7].

ZSM-5 features unique catalytic, shape selectivity, and high stability owing to its unique configuration of linked tetrahedra consisting of 8 five-membered rings (often called a pentasil unit), as shown in Fig.2a. The pentasil unit can connect through edges and extend into a chain structure, as shown in Fig. 2b. The chains then connect through oxygen bridges to form into sheets, and the linking of the sheets through oxygen bridges can develop into a three-dimensional framework of highly ordered arrays [7]. The stacking of the sheets creates two sets of 10-membered-ring (10-MR) channels that are interconnected and run perpendicular in the lattice of the ZSM-5 framework, as shown in Fig.3a. The stack of (010) planes in the y-axis form straight 10-MR channels (elliptical, $5.3 \times 5.6 \text{ \AA}$) running perpendicular to the planes. Then, a set of sinusoidal 10-MR (circular, $5.1 \times 5.5 \text{ \AA}$) is formed in the x-axis parallel to the (010) planes.

Large cavities (ca. 9 Å) are formed at the intersections of the two sets of 10-MR channels, where large molecules may reside [8]. The sheets parallel to (010) and (100) are shown in Fig. 3b, cc.

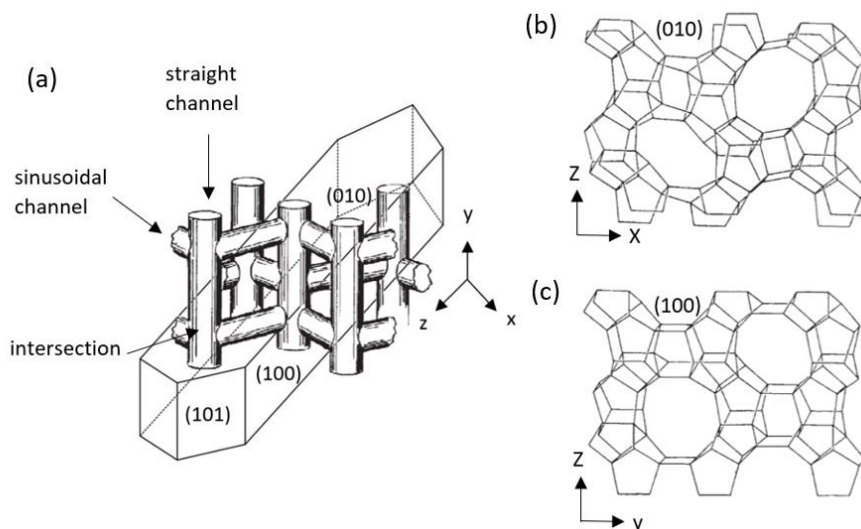


Figure 3. (a) Perpendicular and regular channels in ZSM-5 lattice, the intersections become cages. (b) ZSM-5 sheet (010) from ref.[7], (c) (100) from ref.[7].

Fig.4 shows the highly ordered cavities and channels within the ZSM-5 structure. A cation-exchange center is formed when an AlO_4^- replaces a SiO_4 in the framework. An additional charge is required to neutralize the cation-exchange center to maintain charge neutrality. Protons, alkalis, or alkaline earth metals can fill into the lattice to balance the charge. ZSM-5 exhibits very acidic behavior when the cation exchange centers are filled with protons (H^+) to form Bronsted acid sites (BAS). The acidity is determined by the silica to aluminum ratio (SAR) in the framework, namely, a higher SAR results in a lower acidity.

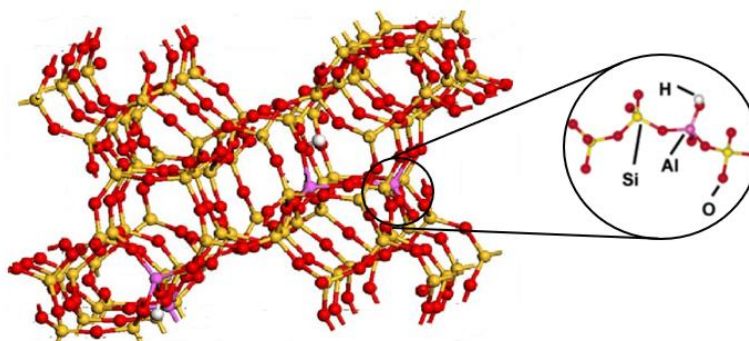


Figure 4. Bronsted acid sites in ZSM-5 lattice from ref.[5].

The crystallographic unit cell formula ZSM-5 is given as:



Where n is a variable that typically ranges from 0 to 27. The total number of silica and aluminum atoms add up to 96 within a unit cell [9]. This implies that the ratio between silicon and aluminum atoms in ZSM-5 lattice can vary over a wide range. Typically, ZSM-5 zeolites have SAR greater than 10. A high SAR makes ZSM-5 zeolite hydrophobic and thermally stable, which are advantageous in many applications [10].

ZSM-5 plays an extremely significant role as a heterogeneous catalyst in the petrochemical industry owing to its acidity, shape selectivity, and thermal stability. The Bronsted acid sites in ZSM-5 frameworks provide a significant extent of catalytic activity in the cracking of hydrocarbons. In conversion of hydrocarbons, the unique pore structures in ZSM-5 framework provide unique shape-selectivity effects favoring the production of product mixture in gasoline range, such as alkenes, light alkenes and aromatic molecules [11, 12], which are valuable commercial products. Some example applications of ZSM-5 include cracking of heavy

hydrocarbons, methane dehydrobromination, methanol to gasoline etc. In China alone, nearly twelve-thousand metric tons of ZSM-5 zeolite are produced annually [13].

1.1.3 Hydrothermal Synthesis of ZSM-5 – Reagents, Nucleation/Growth, and Mechanisms

1.1.3.1 Synthesis and Reagents

Zeolites are typically synthesized under hydrothermal conditions using batch processes. The synthesis precursor typically contains a silicon source, an aluminum source, and a mineralizing agent (most commonly alkali hydroxide) in the presence of a structuring directing agent (SDA) or, in some cases, zeolite seed crystals can be added instead of SDAs to facilitate the crystallization of targeted zeolite structure.

In a typical conventional hydrothermal synthesis (see Fig.5), all reactants are first mixed to form an amorphous zeolite precursor. Then, the reactant mixture is typically aged at ambient conditions or at low temperatures for some time so that the reactants in a fresh mixture can be homogeneously mixed. In addition, dissolution of silica through the hydrolysis of Si-O-Si bonds, polymerization, condensation, and a series of reactions are happened during the aging treatment as well, which result in the formation of local short-range orders that can effectively shorten the induction period for crystallization [14-16]. After the aging step, the synthesis precursor is then heated in a sealed Teflon-lined, stainless-steel autoclave (at temperatures typically below 200 °C) to carry out the synthesis under hydrothermal conditions. In the initial phase of the synthesis, the reactants remain to be amorphous. As the reaction proceeds for a certain amount of time, often called an induction period, zeolite nuclei could be detected, which will then continue growing into larger crystals. Finally, all amorphous precursors will fully transform into zeolite crystals. The reaction time for hydrothermal synthesis can vary between a few hours or several days.

Multiple synthetic parameters can affect the nucleation and crystallization of zeolites. Variations in temperature, synthesis time, alkalinity, ratios between reactants, sources of reactants, water content, stirring, and many other factors could lead to distinct differences in the zeolite formed, crystal size/morphology, chemical compositions, etc.

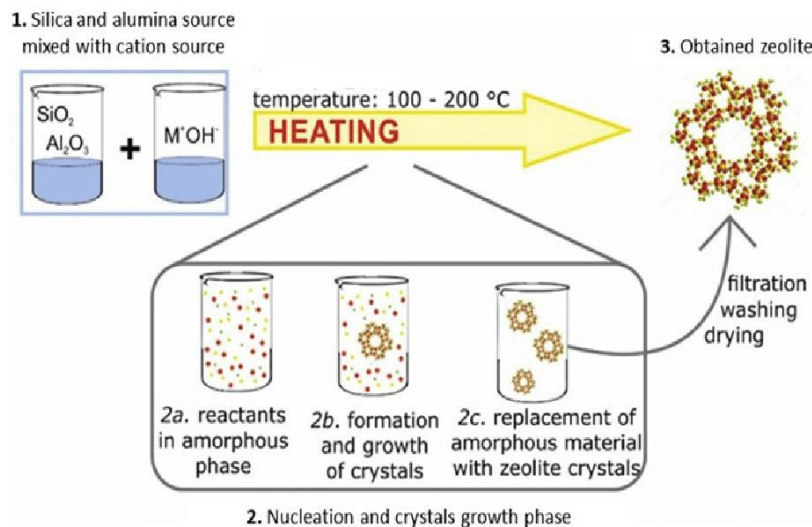


Figure 5. An illustration of general procedures for hydrothermal synthesis in an autoclave from ref.[17].

The choices of starting reagents for hydrothermal synthesis of zeolites are flexible. Common silica and aluminum sources are oxides that contain Si-O and Al-O bonds, such as colloidal silica, tetraethyl orthosilicate for silica, aluminum oxide and aluminum hydroxide for aluminum source. Under hydrothermal treatment, zeolite crystals (e.g., ZSM-5) containing Si-O-Si and Al-O-Si linkage will be readily formed. The mineralizing agent can come from different sources, such as alkali hydroxide (NaOH, KOH, etc.), sodium aluminate, or hydroxide salts of SDA. An alternative source of the mineralizing agent is fluoride-containing salts (HF, NaF, NH_4HF_2 , or NH_4F), resulting in a much lower PH in the reactant solution [18]. The fluoride route has an advantage in synthesizing zeotype frameworks in a neutral or weak basic

environment where the precursor species would be precipitated at higher PH [19]. SDA provides a “templating effect” in hydrothermal synthesis. SDAs usually have a size, structure, or charge distribution commensurate with the composite building units (CBU) or channels and cages of the targeted zeolite, directing the crystallization towards a specific zeolite. SDAs can be categorized as organic (OSDA) and inorganic (ISDA) structure-directing agents. Common ISDAs include alkaline and alkaline earth metals, and they are typically used in the synthesis of low Si/Al zeolites under high pH conditions [20]. On the other hand, OSDAs are often more complex and versatile in structures. Most OSDAs are artificial molecules invented in laboratories with no natural counterparts. OSDA is essential for synthesizing specific zeolite frameworks, especially those with a high silica to aluminum ratio. However, OSDAs are expensive and undergo significant thermal decomposition at elevated temperatures, so crystallization is limited. In addition, the removal of OSDAs from zeolite frameworks by calcination generates polluting gases such as NO_x and CO₂, increasing the cost for both energy and waste gas treatment. These disadvantages of OSDA synthesis possess limitations on industrial production due to economic and environmental considerations. A seed-assisted approach where zeolite seed crystals are added to the synthesis mixture to guide targeted zeolite formation creates opportunities for OSDA-free synthesis [21]. A common hypothesis is that the dissolution of zeolite seed crystals happens in the reactant mixture, creating some shared features, i.e., composite building units (CBU), to guide the formation of daughter zeolite with the common CBUs [22]. A handful of studies have demonstrated the successful synthesis of a variety of zeolite framework using the seed-assisted approach, such as BEA, [23] MFI, [24] MTW [25], etc. [26].

1.1.3.2 Nucleation and Growth

Supersaturation is the driving force for the nucleation and crystal growth in liquid solutions [27], and it is defined as:

$$\Delta\mu = \mu_s - \mu_c \quad (1-2)$$

where μ_s is the chemical potential of precursor solution, and μ_c is the chemical potential of the bulk crystal phase. Nucleation and crystal growth occur when the solution is supersaturated ($\Delta\mu > 0$). Crystal growth reaches equilibrium when the solution is saturated or unsaturated ($\Delta\mu \leq 0$).

The LaMer model [28] (See Fig.6) is a widely accepted model that describes the mixing of particles in a homogeneous solution [29]. Upon the mixing of all reagents, the concentration of precursor solute gradually builds up in the solution over time, creating a degree of supersaturation (Phase I). When the concentration of precursor solute exceeds the critical threshold for nucleation ($C_{nucleation}$), nucleation initiates in the solution (Phase II). The concentration of precursor solute reaches the maximum (C_{limit}) when the rate of precursor dissolution is in balance with the rate of nucleation. Then the level of supersaturation starts to slowly decline as the consumption of precursor solute increases due to the growth of the nuclei. After the concentration drops back below the critical threshold for nucleation (Phase III), the system enters the diffusion growth region where particles continue to grow through addition of precursor solute on to the nuclei, Ostwald ripening and coalescence of nanoparticles. The concentration of the solute continues to be lowered until when the crystal phase is in equilibrium with the solution, then there is no driving force for further crystal growth.

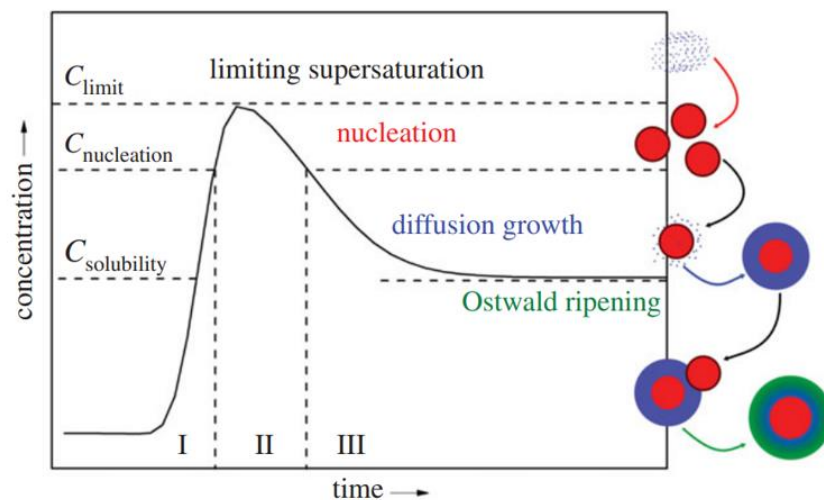


Figure 6. The famous LaMer model of nucleation and growth from ref.[30].

1.1.3.3 Mechanism

The mechanism by which zeolite crystals form during hydrothermal synthesis, as well as possible intermediate structures, are not well understood because of the complex nature of the reaction, with numerous chemical and physical processes, i.e., solution-precipitation, polymerization-depolymerization, nucleation-crystallization, co-occurring and competing [31] [32]. Different mechanisms have been proposed over the years, and most of the advancements have been achieved by the slow accumulation of knowledge and the development of new characterization techniques. Extensive discussions on this topic can be found in the literature [5, 18, 33]. In 1994, Burkett and Davis studied the role of tetra propylammonium (TPA) as an organic structure-directing agent in the hydrothermal synthesis of ZSM-5 zeolite and proposed the formation mechanism for TPA-ZSM-5 (Fig.7). Their work indicated that the crystallization of ZSM-5 involves the prearrangement of silicate species around the TPA⁺ cation, forming into silicate-organic composite structures that later evolve into the channel intersections in ZSM-5 framework. The formation of the silicate-organic composite begins with the clustering of

hydrophobic hydration spheres around TPA⁺ cations. Then silicate species substitute the hydration layer with the release of water molecules due to more favorable der Waals interactions to form into the silicate-organic composites. Aggregation of these silicate-organic composite structures induces nucleation. Then, the nuclei grow into crystals through the addition of the composite structure to the nuclei surface [34].

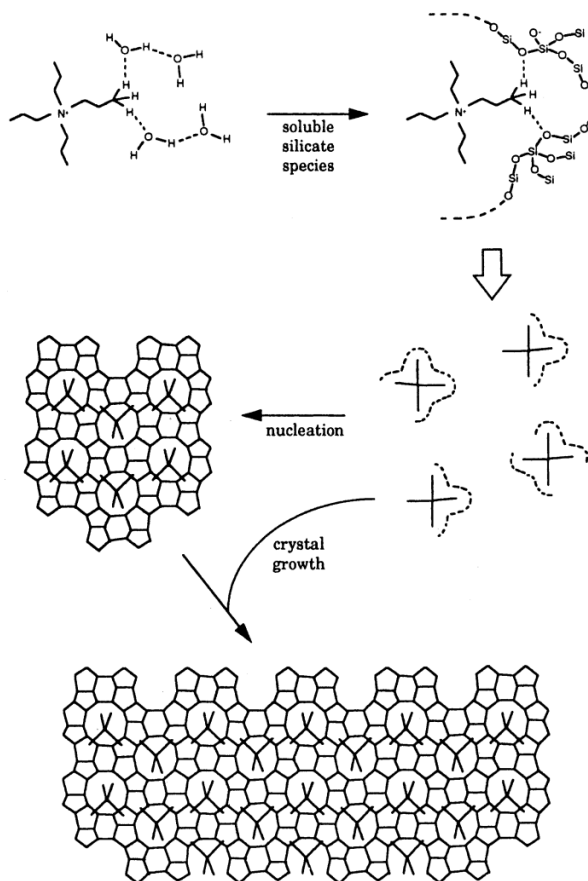


Figure 7. Growth Mechanism of ZSM-5 in the presence of TPA proposed by Burkett (during his PH. D study) and Davis in 1994 from ref. [34].

1.1.4 Transition from Batch Hydrothermal to Continuous Flow Hydrothermal Synthesis

Since the birth of the first synthetic zeolite in the 1940s, up to the present, zeolites have been mostly synthesized under hydrothermal conditions using batch processes. Batch hydrothermal synthesis is a reliable method of converting amorphous reactants into crystalline phases. However, the process itself, typically carried out in batch operation, is inefficient in terms of energy, time, and operation [35, 36]. Batch hydrothermal synthesis of zeolites involves heating the reactants in a PFTE-lined autoclave that is continuously operated at high temperatures ($< 200\text{ }^{\circ}\text{C}$), and at high autogenous pressures for long hours or even days for the synthesis to complete [5, 37]. The continuous heating at relatively high temperatures for a long synthesis period makes the process extremely time consuming and energy intensive. These problems raise concerns in larger-scale production. When batch reactors are scaled up for industrial production, much thicker walls are needed to sustain the high pressure under hydrothermal conditions, which renders the heat transfer even less efficient. On top of that, zeolites are meta stable phases. A variety of synthetic parameters can influence the crystallization and the zeolite frameworks formed. To successfully scale up lab-scale synthesis of specific zeolites, and to achieve controlled production at a large scale, it is crucial yet challenging to match the synthesis conditions in the laboratory. For example, homogeneous mixing and fast heating/cooling are challenging, in industrial equipment [38]. The high costs for equipment, operations, and safety regulations pose limitations on the scale-up of batch hydrothermal synthesis of zeolites for industrial production. Considering the vast demands for zeolites and their wide range of applications, it is highly desirable to develop a fast and efficient synthesis route.

Alternatively, continuous flow processes in existing chemical plants have been proved to be advantageous over traditional batch productions. The advantages of continuous processes may include increased production rate by accelerated kinetics, improved energy efficiency without the frequent start up and shut down operations, more uniform product through readily controlled reaction conditions, less safety concerns, and orders of magnitude smaller system sizes that lowers the capital cost [39-41]. Great emphasis and developments have been achieved in continuous synthesis of organic compounds and polymers for applications in the petrochemical, pharmaceutical, and food industries. In comparison, continuous synthesis of inorganic materials has achieved fewer applications partially due to the process often involving solid reagents/products rendering continuous processes difficult to perform. Among the currently available methods for continuous synthesis of inorganic nanomaterials [42-44], continuous flow hydrothermal synthesis (CFHS) is the most promising method in terms of its potential applications, industrial scalability, and reaction controls [45, 46]. A general scheme of CFHS process is shown in Fig.8. The process generally involves a high-pressure liquid pump which feeds a stream of water at room temperature through an in-line heater to generate superheated water, and then directly mixes with precursor solution from a separate feed in a continuous flow reactor. After the reaction, the product stream is passed through a cooling stage, and then collected as an aqueous slurry after flowing through a back pressure regulator (BPR).

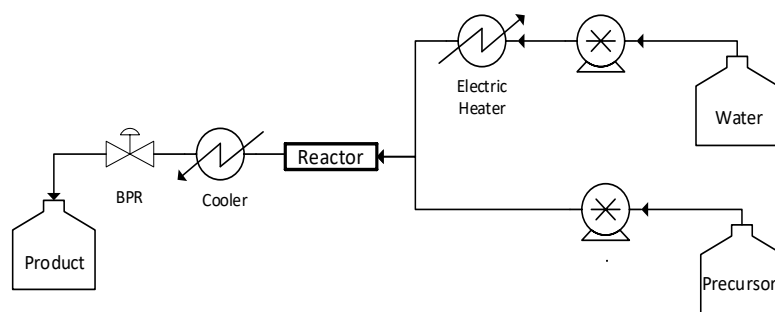


Figure 8. A general schematic for CFHS process.

The idea of continuous hydrothermal synthesis was first introduced in the early 1990s, when Tadafumi Adschiri et.al achieved rapid production of various metal oxide nanoparticles (NPs) in a continuous flow reactor, where a metal salt aqueous solution is directly mixed with supercritical water in a small-sized stainless-steel tubular reactor [46]. The direct mixing generates immediate heating to high reaction temperatures so that hydrolysis could immediately take place, resulting in the formation of NPs within 2 mins. Since then, CFHS has been predominantly studied for metal oxide and sulfide nanoparticles (NPs) synthesis. Numerous studies have demonstrated the advantages of using CHFS over batch hydrothermal methods [45]. With rapidly growing interest in process intensification across the industry, research on CHFS is expanding into new areas such as metal-organic frameworks (MOF) [47-49] and core-shell composite nanomaterials [50].

Despite the development of CFHS is quite recent, there are already successfully scaled-up CFHS processes for commercial production of metal NPs. Hanwha Chemical built the world's first industrial plant for the CFHS of LiFePO_4 in 2011, shown in Fig.9b. The proposed capacity for the continuous plant was 300 tons per year. The Lester Group at Nottingham University partnered with Promethean Particles to construct the world's largest multi-

nanomaterial CFHS process (Fig.9a) in 2016. The plant has a capacity of continuously producing 1000 tons NPs per year. With the grown interest and the recent advancements, CFHS has a bright future towards the fast and efficient production of nanomaterials, composites, and frameworks.



Figure 9. (a) World’s largest multi-nanomaterial Promethean Particles 1000 tons NPs per year 2016. (b) The world’s first commercial CFHS facility for a large-scale production of LiFePO₄ (Hanwha Chemical Corporation). 2011.

1.1.5 Continuous Flow Hydrothermal Synthesis of Zeolites – Opportunities and Challenges

The slow crystallization rate of zeolites is the primary impediment to developing a continuous flow synthesis process due to an associated long residence time. Therefore, improving the crystallization rate of zeolites is critical to make continuous flow processes realistic. A handful of studies in the past have reported that the fast heating in tubular reactor allowed for much-accelerated synthesis of zeolites [51-53], because tubular reactors enable much enhanced heat transfer rate compared to traditional batch hydrothermal reactors. Liu et.al demonstrated the fast synthesis of various zeolites and zeotype materials in a millimeter-sized tubular reactor [54]. The synthesis period of the zeolites and zeotype materials was shortened to

tens of minutes, as opposed to hours or days that are necessary for syntheses conducted in conventional hydrothermal reactor. This is because the heat transfer rate is superior in a small-sized tubular reactor compared to a batch hydrothermal reactor due to a significantly higher surface-area-to-volume ratio, and the fast heating of the zeolite precursor enabled a drastic acceleration of zeolite crystallization kinetics.

The much-accelerated crystallization in a flow reactor opens the door for continuous flow synthesis. Over the years, efforts have been put into developing zeolite synthesis in a continuous flow reactor. Most studies [51, 55, 56] used a HPLC to deliver a precursor solution at room temperature to a tubular reactor that is placed in an oven or immersed in a hot oil bath to heat up the reaction. While different groups have successfully achieved continuous flow synthesis of zeolites using the oven and oil-bath heating methods, these conventional-heating approaches are not the most efficient in heating up the reaction because of thermal lag resulted from indirect heating of the precursor solution from the outside. The slow heating rate requires a longer time to heat up the reaction, and since the residence time in a flow setup is based on the heated volume of the reactor, an exceedingly long reactor is often needed to achieve a sufficient residence time for full crystallization. To achieve a faster heating rate in a tubular reactor, several studies have attempted the application of microwave heating in continuous flow synthesis of zeolites [52, 57, 58]. Microwave irradiation can directly heat up the reaction inside the tubular reactor to accelerate crystal growth. For example, Park et.al demonstrated the application of microwave heating in continuous synthesis of ZSM-5 zeolite, which resulted in a fast crystallization of ZSM-5 within 5 mins in a flow reactor [58]. Even though heating the reaction using microwave has a lower thermal lag effect compared to the conventional heating methods, it would still take some time to heat up the reaction to a high temperature, leaving room for even faster kinetics.

Continuous flow hydrothermal synthesis offers the opportunity to further overcome the limitations of the slow kinetics of zeolites, shortening the residence time owing to its instantaneous heating to a very high reaction temperature achieved by direct mixing of superheated water with the precursor gel. Liu et.al demonstrated the synthesis of ZSM-5 zeolite in a continuous reactor by direct mixing of the zeolite precursor with high-temperature superheated water in a millimeter-sized tubular reactor, where a high temperature (260 °C) can be reached immediately to accelerate ZSM-5 crystallization, and crystallization was able to proceed to complete within only several seconds before the complete decomposition of OSDA under the high temperature [59]. The instantaneous temperature increases to 260 °C (vs. <200 °C in conventional batch synthesis) generated by the directing mixing of the two feeds significantly accelerated the crystal growth, pushing crystallization to complete in just a few seconds, which is in stark contrast to tens of hours or even several days that is required for conventional batch synthesis. The instantaneous increase to very high temperature is a key factor responsible for the successful synthesis of zeolite in a vastly shorter period of time. However, careful considerations should be taken when designing the reaction conditions to match the kinetics with thermodynamics. Zeolites are metastable phases under hydrothermal conditions. Formation of undesired dense-phase counterparts may happen at an overly high reaction temperature. In addition, decomposition of OSDA is enhanced at higher temperatures due to its low temperature stability. Therefore, any single-minded efforts trying to achieve faster kinetics by blindly increasing the crystallization temperature will be ineffective.

The second major challenge for developing a continuous flow reactor for zeolite synthesis is the formation of zeolites as solid particles in a high concentration behaving like a slurry. The sedimentation of solid particles and fouling in a continuous process can happen

within different reactor components (mixing element, tubular reactor, BPR, connectors) which easily lead to an incorrect residence time for various product streams and eventually blockages. Common approaches to avoid accumulation and blockage in tubular reactor section include the use of “non-stick” materials and the application of external forces such as mechanical agitation. For example, Liu et.al used a pneumatic vibrator to agitate the reactor to minimize particle sedimentation and blockage [59]. A handful of groups reported on the use of specially designed reactors that manipulate hydrodynamics to minimize precursor-wall contact. ‘Fouling-free’ can be achieved in a focusing flow reactor (see Fig.10a) where the reagent flow stays in the core and the reactor wall is shielded by a ‘sheath’ flow against fouling [60, 61]. The Lester group designed a counter-current mixing reactor featuring a pipe-in-pipe design (see Fig.10a) [62, 63]. Superheated water is injected from an inner pipe (downflow) into a precursor stream (up flow), achieving a uniform mixing profile that is effective in preventing the aggregation of metal oxide NPs at the mixing point. To avoid particle aggregation that happens at the mixing point, many groups have also demonstrated the use of non-traditional tee-mixers, such as swirling micro mixers (see Fig.10d) for improved mixing efficiency hence reduced particle settling [64, 65]. Another way to address the challenge of solid precipitation and fouling in a continuous flow reactor is to utilize a segmented flow (see Fig.10e). Segmented flow is created by dispersing a precursor in an immiscible surfactant to form into microdroplets, so that a smooth and continuous flow of solid products in the form of suspension can be achieved in a flow reactor [66]. Besides reactor fouling, a high concentration product slurry can also lead to clogging and failure of the back pressure regulator as conventional BPR vulnerable to blockage by particulate flows due to small-bore components. General approaches to avoid BPR failure are achieved through dilution of the slurry flow [59], employment of two filters and BPRs in parallel to allow

continuous operation [49] or development of novel methods. For example, Deadman et.al developed a pressure chamber where product slurry is collected in a vessel pressurized by gas (see Fig.10.d) [67]. The product collected in the pressurized vessel is retrieved after the synthesis.

The continuous hydrothermal synthesis of zeolites brings a fast and efficient route for industrial production. Meanwhile, the complexity of zeolite formation makes continuous flow synthesis of zeolites a challenging task. Only a comprehensive strategy taking the various challenges (kinetics, thermodynamics, hydrodynamics) into consideration will make a continuous flow synthesis of zeolites possible.

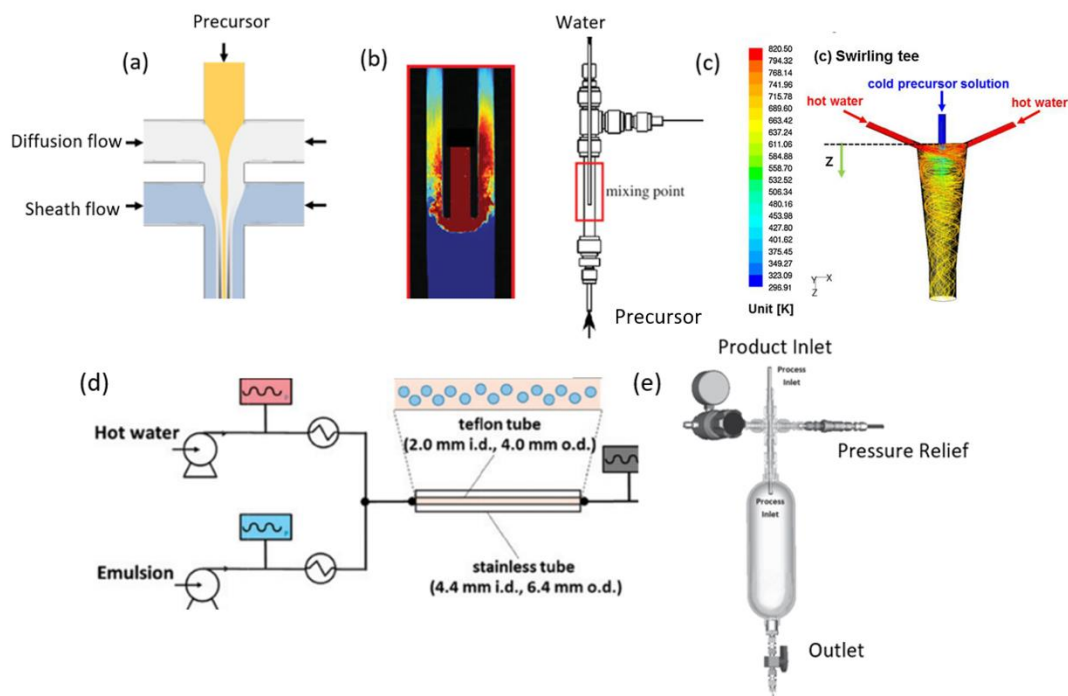


Figure 10: A schematic showing designs of different reactor components in CFHS process. (a) A ‘fouling-free’ focusing flow reactor where the reactor wall is shielded against the reagents stream by the ‘sheath flow. The diffusion flow prevents the precursor from the core from meeting the ‘sheath’ flow at walls [61]. (b) Countercurrent mixer designed by Lester Group [62, 63]. (c) Computational fluid dynamics simulation result of a swirling tee showing a turbulent mixing regime[65]. (d) Segmented flow setup where the precursor is dispersed in oil to form an emulsion phase and then mixed with the hot water into the reactor [66]. (e) A pressure chamber acts as a BPR where product slurry is collected in the chamber. The chamber has a maximum 1L capacity and can safely handle temperatures up to 140 °C and 10 bar of pressure [67].

1.2 Project Objectives

Current batch-mode production of ZSM-5 zeolite takes a lengthy period of hydrothermal treatment (high T & P), which is highly inefficient in terms of time, energy and operation when considering a large-scale production. Given the large demand for ZSM-5 zeolite and its diverse range of applications, a fast and efficient synthesis process is attractive.

This work seeks to develop a continuous flow hydrothermal process for the synthesis of ZSM-5 with vastly accelerated synthesis times and a high production rate. The approach is based on the direct mixing of the zeolite precursor with high-temperature superheated water in a millimeter-sized continuous flow reactor, where high temperatures can be reached immediately to accelerate ZSM-5 crystallization.

To achieve this goal, the work is broken down into the following objectives:

Develop a continuous hydrothermal flow synthesis system for ultrafast synthesis of ZSM-5 zeolite for lab use

Study the effects of temperature and residence time on crystallization to achieve highly crystalline materials

Optimize the system to increase run time and production rate

1.3 Outline of the Thesis

Chapter I provides background information on ZSM-5 zeolite, including its structure and properties, the synthesis reagents, theory of nucleation and crystal growth mechanism.

Background information on CHFS, limitations of batch hydrothermal synthesis, motivation, challenges for developing a CHFS for ZSM-5 synthesis and the main objectives of this research.

Chapter II provides detailed explanations on the continuous setup, experiment procedures, preparation of synthesis materials and material characterizations.

Chapter III presents the important results of this work and relevant discussions.

Chapter IV draws the conclusion and provides future directions for research.

2.0 Materials and Methods

2.1 Materials

The following materials were used: colloidal silica (LUDOX AS-40, 40 wt. % suspension in H₂O), aluminum hydroxide (≤ 100 %, Sigma Aldrich), sodium hydroxide (NaOH, pellets, 98%, Alfa Aesar), TPAOH (40wt% aqueous solution, Sigma Aldrich) and iron (III) nitrate nonahydrate (99.95%, Sigma Aldrich).

2.2 Preparation of Synthesis Mixture for ZSM-5

The synthesis recipe is adopted from a prior published work [59]. The synthesis mixture had a composition of 150 SiO₂: 1 Al (OH)₃: 10 TPAOH: 25 NaOH: 1150 H₂O, and it was prepared as follows: Half of NaOH was first dissolved in deionized water to prepare an aqueous solution (10 wt.%). The as-prepared NaOH aqueous solution (10 %) was then added to colloidal silica and stirred for 30 minutes. The other half of NaOH, TPAOH, and Al (OH)₃ were mixed and stirred for 5 minutes. Next, the two mixtures were combined and stirred for another 30 minutes. Lastly, the final mixture was aged at 90 °C in a sealed Teflon-lined stainless-steel autoclave, followed by an aging treatment carried out in a rotating oven at 20 rpm for 16 hours.

2.3 Batch Hydrothermal synthesis

Reference materials were synthesized using the same recipes in conventional hydrothermal reactors following the aging step. Without taking out the synthesis mixture from Teflon-lined stainless-steel autoclave after the aging step at 90 °C for 16 hours, the oven temperature was elevated to 170 °C to carry out hydrothermal treatment for 24 hours while rotating at 20 rpm. The product obtained was washed with deionized water and dried overnight in a vacuum oven at room temperature, followed by calcination at 550°C in air for 5 hours.

2.4 Design and Setup

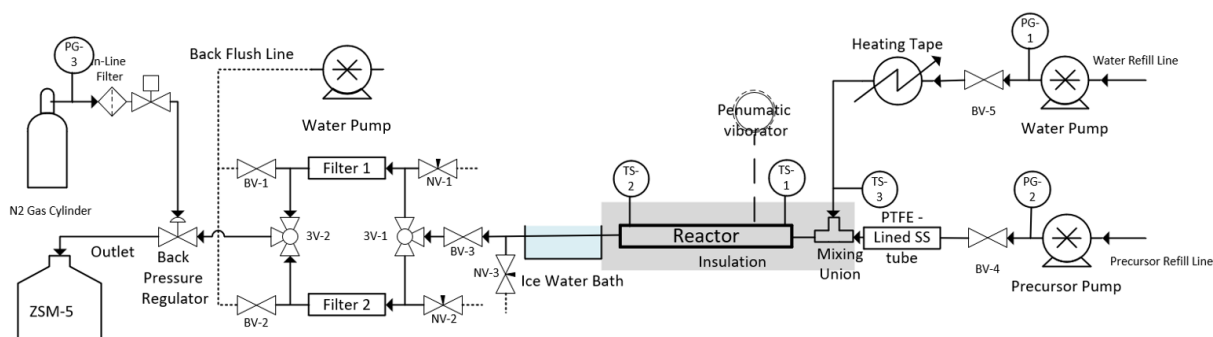


Figure 11. A detailed schematic showing the full continuous synthesis setup.

The continuous synthesis setup includes the following components: high pressure positive displacement pumps (ISCO, 100D for the Precursor pump, ISCO, 500D for the Water and the Back-Flush Pump), temperature controller (Omega), compressed air-driven vibrator (Netter NCT-2), back pressure regulator (Equilibar, ZF-1SNN8), temperature sensors (Omega, CS8DPT), filter upstream BPR (Swagelok, SS-8F-40, strainer type), heating tape (omega),

pressure transducer (ISCO, TJE), pump controller (ISCO, D series), All tubing, fittings and valves that were used in building the system are standard-off-the-shelf stainless steel parts (Swagelok). Please see Fig.S1 – Fig.S4 for detailed illustrations for the setup.

In the continuous synthesis setup, water via a high-pressure syringe pump is heated in the process to become superheated and is pumped to a T mixer, where it meets the room temperature precursor gel from another high-pressure syringe pump. Direct mixing of room temperature precursor gel and high temperature, superheated water in a continuous flow reactor generates instantaneous heating to high temperatures so that ZSM-5 crystallization immediately takes place. After the reaction, the product stream is rapidly quenched down to a sufficiently low temperature by an ice water bath to minimize the decomposition of organic structure-directing agent (OSDA) and to avoid the formation of dense-phase zeolite counterpart. The product is collected as an aqueous slurry after passing through the back-pressure regulator. The inline filters protect the downstream BPR from large solid particles. Two sets of filters are installed in parallel to achieve a continuous operation. A backflush pump flush deposited particles out of the filters with water at high flow rates from downstream, and the aqueous slurry flushed out of the filters are collected as product as well. A compressed air-driven vibrator is mounted onto the reactor to minimize precipitation or blockage problems. The precursor feed line is Teflon-lined to reduce fouling via ‘pre-crystallization’ and attachment of any residual “pre-crystallized’ product to the tube walls.

2.5 Continuous Synthesis

In a typical operation, all pumps were initially filled with deionized water. The set-point reference pressure was set to 100 bar for the back pressure regulator. The system was gradually pressurized and preheated to target temperatures by running water. After the temperature and pressure in the system stabilized, precursor gel was refilled into the precursor pump. While refilling the precursor, the heater and the water flow halted. Once refilling was done, the process resumed, and the synthesis began. The flow rates for precursor gel and water were kept at 4 ml/min and 16 ml/min, respectively, which mixed to a temperature of 276 °C in the reactor. The compressed air-driven vibrator operated at 200 Hz under 15 psi. Considering the density of water at 276 °C to be 750 kg/m³, the actual flow velocity in a ½ inch tubular reactor (with an ID of 10 mm) is ~ 0.054 m/s, which means the length required for a residence time of 75 s is 40 cm. The system pressure and reactor temperatures were recorded every minute. The product flow was allowed to pass through filter 1. When filter 1 started to clog (as indicated by an increase in upstream pressure), the three-way valves (3V-1 and 3V-2) were switched to direct the flow into a clean Filter 2, allowing the operation to proceed further. At the same time, a backflush pump was used to clean the deposited particles out of Filter 1. Once Filter 2 started to clog, the three-way valves were switched back to Filter 1 to allow continuous production. The aqueous slurry flushed out of the filters was collected. When synthesis was finished, the heater and the precursor pump were turned off whilst water continued to flow to cool down the system. After the system had been cooled, the water pump and the vibrator were turned off. Then, the ball valve (BV-3) was closed, and the system pressure was reduced through the releasing needle valve (NV-3). The drainage from the system containing a high solid content was collected. Thereafter, the pressure

left after the BV-3 was released, and the filters were removed from the system to retrieve the deposited particles in the filters. Finally, the system and the precursor pump were disassembled to clean out any deposited particles. The aqueous slurry collected at the outlet during the synthesis, the particles flushed out of the filters during the synthesis, the deposited particles in the filter retrieved after the synthesis, and the residue cleaned out from the system, were separately centrifuged, washed, dried, and calcinated at 550°C in air for 5 hours to collect final ZSM-5 product. At a precursor flow rate of 4 ml/min, the production rate at the outlet was 0.41 g ZSM-5/min, which equals 590 g/day, assuming a continuous synthesis.

2.6 Computational Fluid Dynamics Modelling

A computational fluid dynamics (CFD) simulation on the mixing zone was developed to study the mixing behavior of the two steams, which is critical for developing the process. The model was using the finite element analysis method in the stationary study in COMSOL Multiphysics 5.6 by using non-isothermal coupled Multiphysics configuring with heat transfer in fluids and laminar flow module. The model was solved using the finite element analysis method, the element was set to normal, and meshing was set to physics controlled. The typical time that a simulation takes for a simulation to converge is around 5 mins. Wat Water was substituted for precursor gel in the simulation due to the difficulty in defining the material properties of which are sensitive to the large temperature change in the system. The dimensions of the physical model were based on the T mixing union (1/4'') from Swagelok Inc.

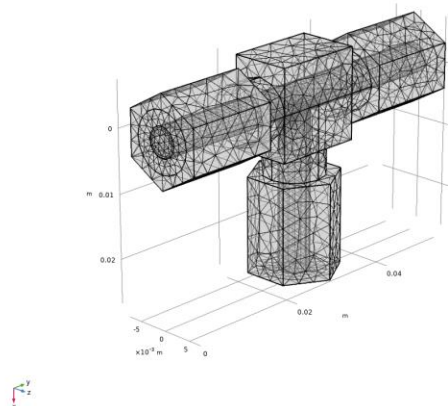


Figure 12. A demonstration of the 3D tee-mixer (1/4") built in COMSOL Multiphysics.

2.7 Zeolite Characterization

2.7.1 X-ray Powder Diffraction and Relative Crystallinity

A Bruker D8 Discover X-ray diffractometer was used to collect X-Ray diffraction (XRD) under 40 mA and 40 keV with Cu radiation under 40 mA and 40 keV. The weight sample was fixed at 9 mg and the diffraction patterns were recorded with a step of $0.02^\circ(2\theta)$, 0.4 sec/step.

The relative crystallinity of ZSM-5 samples was calculated as the proportion of the absolute height of the peak centered at around 23.1° of the sample ZSM-5 and reference ZSM-5. A baseline is constructed from the center of the background scatter at 21.2° to the center of the background scatter at 25.0° on the XRD patterns.

$$\text{Relative Crystallinity} = \frac{\text{peak height for the sample}}{\text{peak height for the reference}} \quad (2-1)$$

2.7.2 Electron Microscopy

A Zeiss SIGMA VP field emission scanning electron microscope (SEM) was used to determine the morphology of ZSM-5 samples at a 3 kV beam voltage. High-resolution transmission electron microscopy (HRTEM, JEOL-2100) was used to determine nanoscale morphology. The elemental composition of ZSM-5 samples was determined using energy dispersive X-ray spectroscopy (EDX) coupled to the scanning electron microscope (SEM; Zeiss SIGMA VP), with a total count collection of 50,000.

2.7.3 Surface Area

A Micromeritics ASAP 200 was used to determine the surface area (S_{BET}) by N_2 adsorption isotherm. Before adsorption, Na-ZSM-5 product was converted into H-ZSM-5 by ion exchange with aqueous NH_4NO_3 solution (1 M) at 80°C for 15 h. Finally, the material was dried under vacuum and calcined at 500°C in air for 5 h. Then degassed at 300°C for 24 h, prior to the adsorption experiments.

2.7.4 Yield

The yield of zeolite is calculated as the weight of calcined product divided by the weight of Al_2O_3 and SiO_2 in the precursor feed.

$$\text{Yield of Zeolite} = \frac{\text{weight of the calcined product}}{\text{weight of } \text{Al}_2\text{O}_3 \text{ and } \text{SiO}_2 \text{ in the initial gel}} \quad (2-2)$$

3.0 Results and Discussions

3.1 Mixing Efficiency in Different Configurations

In continuous flow hydrothermal synthesis, the mixing between precursor gel and superheated water is crucial to the process. The importance of rapid mixing of the two feeds is several-fold. First, it allows rapid heating of the reaction to a high temperature to accelerate crystal growth. Second, a uniform mixing results in a homogeneous reaction condition and hence uniformity in the zeolite crystals formed [68]. Third, a strong mixing effectively prevents the gel particles from aggregation at the mixing point to cause blockage in the tubular reactor. The use of stainless-steel parts in the system, which was constrained by high-temperature and high-pressure conditions, made visualizing the mixing behavior of room temperature precursor with superheated water, which are at hugely different temperatures, densities, and viscosities, impossible. In this case, computational fluid dynamics (CFD) serves as a powerful yet convenient tool to study the mixing behavior of the two feeds inside the T-piece mixer.

There are three possible configurations to mix the precursor gel, and the superheated water in a T-piece mixer based on the direction of the feed flows relative to the mixing point. To compare the mixing efficiency when mixing precursor gel and superheated water in different configurations, a CFD model was employed to calculate the mixing profile in each of the cases, and the results are shown in Fig.13. When superheated water is fed from the right, and room temperature precursor gel is mixed from the bottom (Fig.12a), a two-phase flow behavior can be clearly observed in the parallel tube after the mixing point. The superheated water, which is at a much higher flow velocity, lower density, and lower viscosity, ‘pushes’ the room temperature

precursor gel to the wall. As a result, the dense precursor gel flows along the bottom side of the parallel tube after mixing, and the interface between the two flows mixes very slowly down the tube. In this mixing configuration, a blockage is more likely to happen due to the poor mixing regime and undesired accumulation of precursor gel in the pipe. Whereas, when superheated water is injected from the bottom and precursor is mixed from the right, a relatively uniform mixing profile can be observed (Fig.12b). After the mixing point, superheated water flows at the center of the tube, then quickly mixes with precursor gel. In symmetrical mixing (Fig.12c), where precursor gel and superheated water are fed on the opposing side to the mixing point, the precursor gel flows to the left side of the vertical tube and gradually mixes with superheated water as it flows downward in the vertical tube. While the latter two scenarios show a similar mixing profile, a closer investigation showed that injecting the hot water at a right angle to the precursor stream resulted in a more homogeneous temperature distribution in the mixed stream. The minimum and maximum temperatures at equally spaced cross-sections of the mixed stream are indicated in the figure. One can see that the minimum temperatures at the different cross-sections of the ‘side-injecting’ scenario are higher than those observed with symmetrical mixing, an indication of a more homogeneous mixing profile.

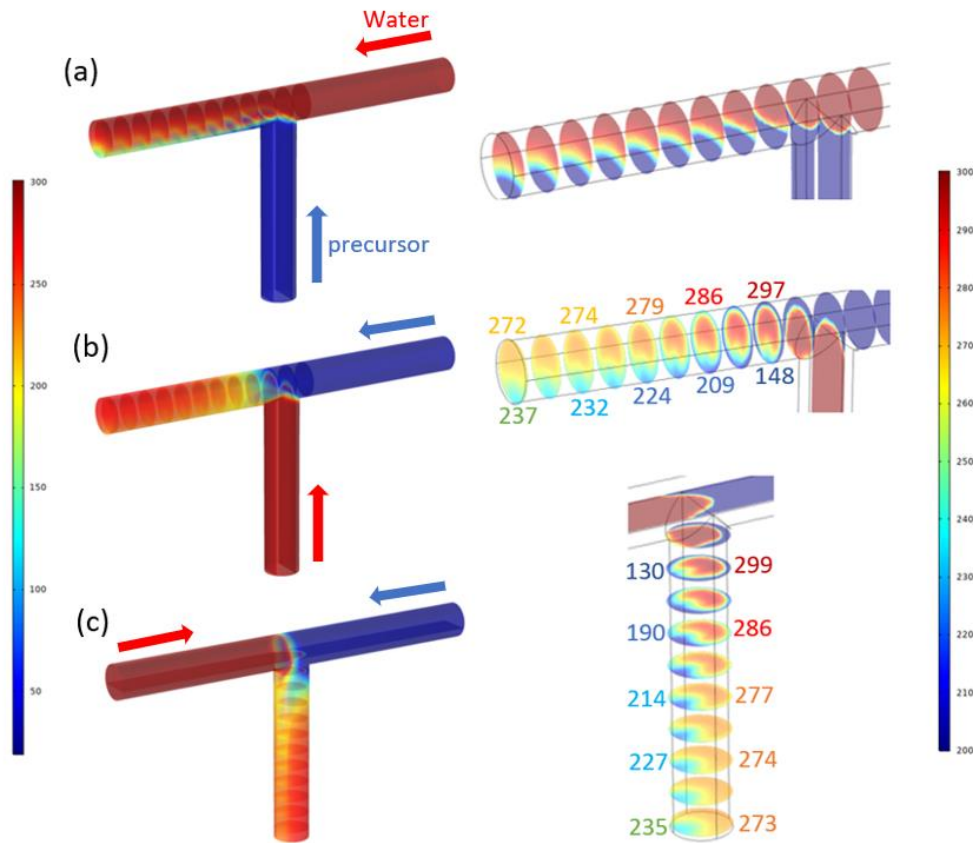


Figure 13. Temperature profile of the mixing between precursor at 4 ml/min, 25 °C, and hot water at 16 ml/min, 300 °C in a 1/4” T mixer in different configurations (a): injecting precursor from the bottom, (b) injecting hot water from the bottom, (c) symmetrical mixing of precursor and hot water. Radial temperature distributions are shown every 0.244 mm downstream of the mixing point in (b) and (c).

The mixing between precursor gel and superheated water is crucial to process. By analyzing the temperature profiles of the mixed flow in different mixing configurations in a T-piece mixer through CFD simulations, it is evident that injecting the superheated water at a right angle to the precursor flow produces the best mixing regime in a T-piece mixer. Notwithstanding, the simulated temperature profiles also show that the T-piece mixer does not provide uniform mixing of the two streams regardless of the mixing configurations. While it is simple to use a T-piece mixer as it is off-the-shelf which can be easily replaced when needed, for

future studies, future efforts should be put into designing and engineering a mixing unit that is best for this process considering the flow rates, temperature, heat exchange, buoyancy/momentum of the mixing stream, etc. via CFD modeling and experimentations to optimize the mixing efficiency.

3.2 Undesired Preheating of the Precursor gel

The direct mixing between room temperature precursor gel and superheated water in the reactor causes the precursor gel to undergo significant preheating before meeting the superheated water. Preheating of the precursor gel is primarily driven by heat conducted from the hot reactor zone back into the gel feed line through metal tubing. Preheating of the precursor feed leads to ‘pre-crystallization’ of zeolite and undesirable accumulation of solid particles in the feed line, resulting in rapid blockages. To confirm the effect of heat conduction, a CFD model was employed in which the temperature profile at the mixing zone could be studied.

Tubing materials with different thermal conductivity were applied in the precursor line to understand the significance of heat conduction on its temperature. Fig.14 demonstrates the difference in temperature profile in the precursor feed line when stainless steel and ceramic tubing are applied in the line. At the same flow conditions, the heat conducted from the hot zone through the stainless-steel tube significantly raises the temperature of the precursor stream by about 100 °C before it meets the superheated water (Fig.14c), whereas the ceramic tube (with a much lower thermal conductivity) could effectively prevent heat from traveling into the precursor feed. The result indicates that the heat conducted into the precursor stream through stainless-steel walls is the leading cause for the ‘pre-crystallization’ of zeolite in the feed line,

which led to rapid blockage of the precursor feed. It is evident from the simulation results that moderating the heat conduction to the precursor line is critical to address the precursor accumulation and the blockage issue.

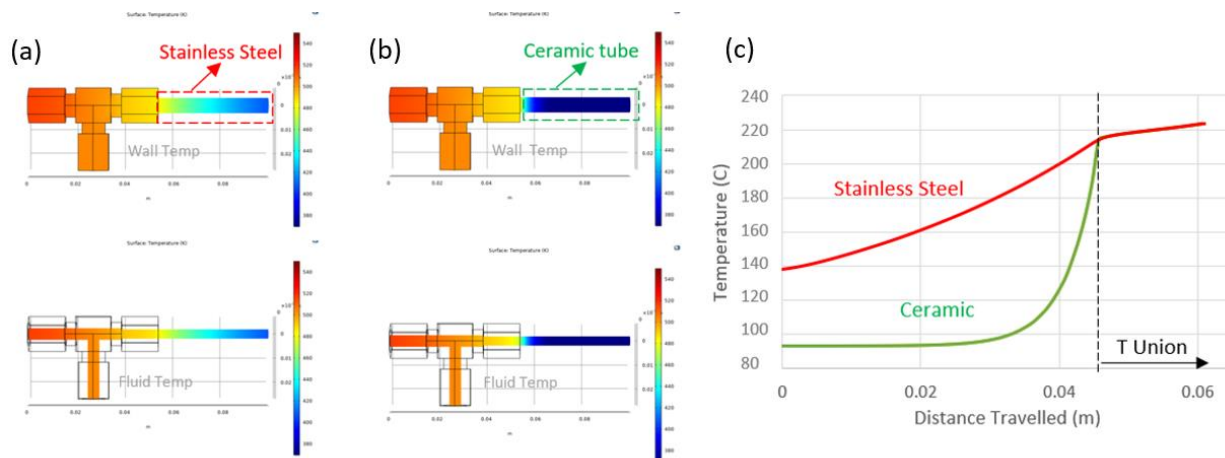


Figure 14. COMSOL simulation results of mixing water at 1 ml/min, 280 °C and precursor at 0.8 ml/min, 90 °C in a 1/4" T mixer in steady state. (a) Temperature gradient plot at the outer wall and fluid surface using stainless steel pipe in the gel feed line. (b) using ceramic pipe in the gel feed line, (c) comparison of precursor temperature when flowing towards the mixing point.

More simulations were done to evaluate different approaches for lessening the effects of heat conduction on preheating of the precursor stream. Increasing the precursor flow rate was found to lower the preheating (through convective cooling), which conceivably has the additional benefits of preventing particle settling and accumulation within the feed line. Mixing precursor and hot water in the different configurations (as discussed in section 4.1) showed insignificant influences on the amount of heat conducted back into the precursor feed.

Numerous approaches were tested in efforts to resolve the blockage in the gel feed line. A piece of ceramic tubing, which is suitable for the synthesis conditions (high temperature and

pressure), was added into the gel feed line. However, the ceramic tube fractured easily due to the expansion of metal fittings upon heating and the vibration from the vibrator. An alternative route was to add a Teflon inner tube to the precursor feed line. Teflon-lining the precursor feed line was effective in preventing blockage of the line, likely due to two simultaneous effects: The Teflon lining is a poor heat conductor, reducing the undesired pre-heating and hence the degree of 'pre-crystallization' of the gel while at the same time reducing attachment of any residual pre-crystallized product. The feed flow rate of precursor gel was increased fourfold to lower the preheating. With a combination of the Teflon-lining and increased precursor flow rate, the blockage issue caused by the preheating was successfully resolved in the system.

CFD modeling was used to confirm the effect of heat conduction on preheating the precursor stream. It is evident that moderating the heat conduction to the precursor line through metal tubing is critical to address the precursor accumulation and the blockage issue. By Teflon-lining the precursor feed and quadrupling the feed flow rate, the blockage issue caused by the preheating was successfully resolved in the system.

3.3 Effect of Reactor Fouling on Conversion

In the continuous flow reactor, zeolites are formed as solid particles, which can then accumulate on the inner reactor surfaces, resulting in reactor fouling. As shown in Fig.15, uniform deposition of zeolite particles happened radially across the surface of the tubular reactor in the form of scale. In a small-bore tubular reactor, deposition of comparable size to the flow channel can happen, disrupting the flow patterns, reducing the inside diameter thus ill-defined

residence times for the reaction stream, resulting in lower productivity, decreased conversion, and eventually complete blockage in the reactor.



Figure 15. A photo showing the fouling observed in a $\frac{1}{2}$ ” tubular reactor after a synthesis at ~ 280 C for 20 mins.

The initial version of the continuous synthesis setup used a millimeter-sized flow reactor made of stainless-steel tubing (OD = 0.125”, ID = 0.069”) based on two considerations. The first was that the millimeter-sized reactor has a high heat transfer rate, allowing for efficient heating to high temperatures upon mixing precursor gel with hot pressurized water [57]. The second reason was to feed small flow rates (precursor: 1 ml/min, superheated water: 1.6 ml/min) to allow a fast and efficient cooling of the reactant flow to minimize OSDA decomposition.

In running the continuous synthesis, the millimeter-sized reactor was found to be highly susceptible to reactor fouling due to its highly small-bore passage. Even a scale deposition of 0.25 mm on the reactor surface will reduce the reactor volume by half. Continuous synthesis was carried out at 150 °C, 200 °C, and 240 °C in a $\frac{1}{2}$ ” tubular reactor. During the synthesis at 240 °C, a rapid blockage happened inside the tubular reactor (Fig.16a) shortly after running the synthesis. Little to no solids were collected at the reactor outlet, indicating a significant degree of

accumulation of solid particles in the flow reactor. Fig.16b shows the XRD pattern of the products collected during the syntheses at 150 °C and 200 °C. It is demonstrated that the crystallinity of the product synthesized at 200 °C is lower than that of the product synthesized at 150 °C, which is not as expected since the zeolite crystallization rate increases with increasing temperature. The SEM images on the two samples are shown in Fig.16c. Both samples are poorly crystallized, but the unconverted precursor particles at 200 °C, on average, are larger in size than those at 150 °C, indicating a lower degree of conversion despite a much higher synthesis temperature. One possible reason for this observation is the worsened reactor fouling at a higher temperature; that is, higher temperatures accelerate the crystallization of zeolites and particle attachment on the reactor surface, resulting in an ill-defined residence time for the reaction stream, and hence a decrease in conversion. In fact, as mentioned earlier, a high enough temperature led to the rapid blockage of the reactor.

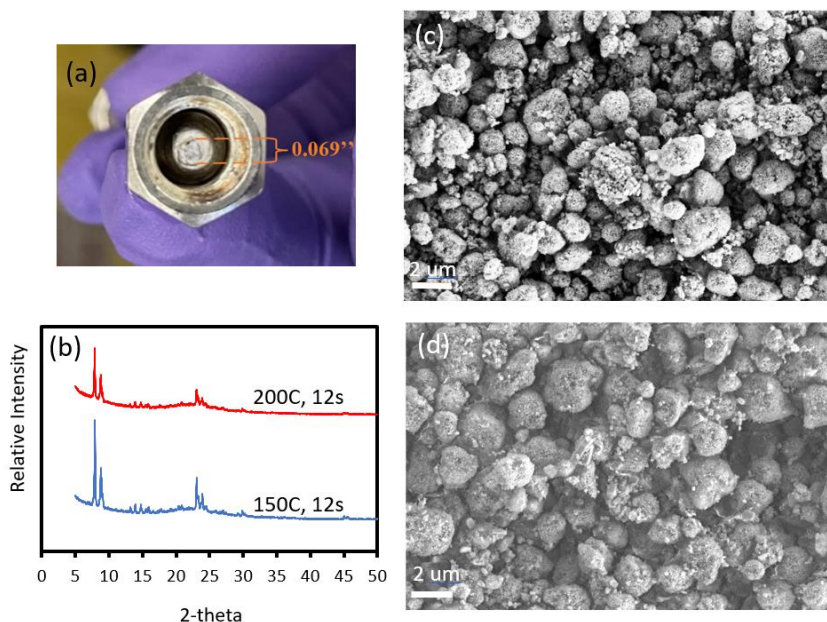


Figure 16. Characterization results of products obtained from continuous flow synthesis in a 1/8'' tubular reactor at different temperatures in 12 s. (a) A photo showing the blocked tubular reactor after a synthesis

carried out at 240 C. (b) XRD patterns of the samples obtained at 200 C and 150 C. (c) SEM image of the sample obtained at 150 C, (d) SEM image of the sampled obtained at 200 C.

To reduce the effect of reactor fouling on ill-defined residence time, the reactor (including the mixing unit) was increased from $\frac{1}{8}$ '' to $\frac{1}{4}$ '' diameter tubing (OD = $\frac{1}{4}$ '', ID = 0.18'') with a larger-bore passage. Fig. 17a shows the XRD patterns of the products obtained from the continuous flow reactor in a $\frac{1}{4}$ '' reactor at different synthesis temperatures. As expected, the product crystallinity increased along with increasing the crystallization temperature. The SEM images (Fig.17b, c) of the samples clearly show much-increased sizes of ZSM-5 crystals as well as decreased sizes of precursor particles at 244 °C compared to 233 °C, indicating a higher degree of crystallization at the higher temperature.

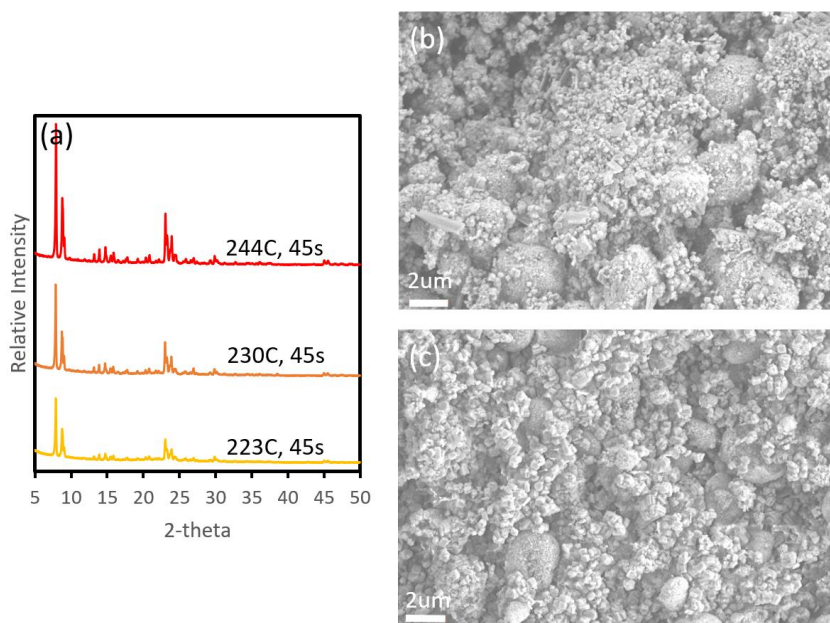


Figure 17. Characterization results of products obtained from continuous flow synthesis in a 1/4'' tubular reactor at different temperatures in 45 s (a) XRD patterns of the samples obtained at 223 C and 230 C and 244 C (b) SEM image of the sample obtained at 223 C, (c) SEM image of the sampled obtained at 244 C.

Increasing the reactor diameter is a straightforward way of reducing the effect of reactor fouling. However, even with a larger flow channel, fouling still poses significant problems. For example, large aggregates might disturb the reactor flow affecting the product quality, and even detach and block the downstream tubing. Furthermore, fouling also lowers productivity (which will be discussed in section 4.7).

3.4 Heat Loss and Temperature Control

The instantaneous heating to a very high temperature is a key factor responsible for the successful synthesis of zeolite in a vastly shorter period of time. The system was designed to directly mix precursor and hot water to enable the rapid temperature increase. After switching to a $\frac{1}{4}$ '' reactor (including the mixing unit) in an effort to reduce the effect of fouling as discussed in the last section, the much-increased size of the reactor and connectors (both of which are made of stainless steel) subjected the system to a more significant heat loss. The low flow rate (of 1.6 and 1 ml/min for water and gel, respectively) loses its heat quickly through the reactor wall as the amount of thermal energy stored in the hot flow is proportional to its volume. Especially at longer residence times (which means longer reactor lengths), the temperature drops across the reactor became significantly large. In addition, the iced-water bath at the downstream reactor acts as a large heat sink, sucking in a massive amount of heat from the hot reactor zone.

In this case, increasing water temperature (through heating) is not ideal for achieving a higher reactor temperature. That will intensify the undesired preheating of precursor gel by conduction through metal tubing, as discussed in section 3.2. A second-staged heating (through heating tape) was applied. Heat loss in the mixing zone and secondary heating led to a much

slower temperature increase compared to a directing mixing scenario, which might worsen the reactor fouling because crystallization is accelerated on the metal surface, which is at the highest temperature. perfect direct mixing scenario, which enhances the decomposition of which enhances the decomposition of OSDA due to a wide time window of high-temperature exposure. In addition, the secondary heating directly heats the reactor from outside, which might worsen the reactor fouling because crystallization is accelerated on the metal surface.

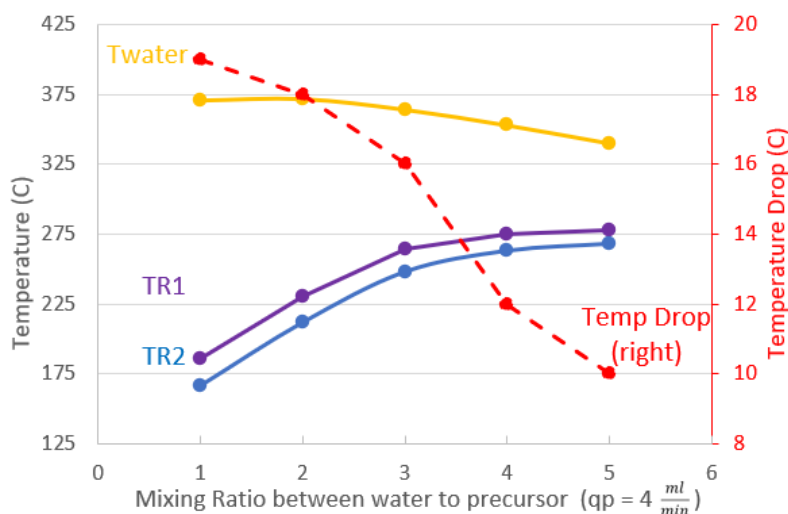


Figure 18. Temperatures in the system measured when mixing precursor at 4 ml/min, 25 °C with water at different flow rates. The temperature of water decreases as the flow rate increases due to insufficient heating. TR1 is the temperature measured right after the mixing union, and TR2 is the temperature measured at reactor exit (see Fig.S2 b). Temperature drop is the difference between TR1 and TR2.

A better approach to achieve desired reactor temperatures would be to increase the hot water flow rates. At higher flow rates, convective heat transfer dominates the temperature profile and lowers the effect of heat loss on reactor temperature. Fig.18 shows the reactor temperature after the mixing zone when precursor gel (at 4ml/min) and hot water are mixed at different ratios. Mixing between water (at 16 ml/min) and precursor (at 4ml/min) enabled reaching the

target reactor temperature of ~ 275 °C. As expected, the temperature drop in the reactor decreases with increasing the hot flow rate. In addition, increasing the precursor flow rate allows for higher throughput (higher yield) and reduces the preheating of precursor feed by convective cooling, which is the main cause for ‘pre-crystallized’ particle accumulation and precursor line blockage (as discussed in section 3.2). Reactor volume needs to be scaled up proportionally to achieve similar residence time. Hence, the reactor diameter was increased further from $\frac{1}{4}$ ” to $\frac{1}{2}$ ” to keep the reactor compact.

Directing mixing to target temperatures was achieved by increasing the hot flow rate. Achieving higher temperature by increasing the flow rates is better than simply increasing the water pre-mixing temperature or employing a second staged heating for several reasons. There is no one size fits all solution for solving the problems. It is important to keep in mind that changing the reactor size and flow rates also means that the flow regime, temperature profile, mixing profile, fluid properties, etc., all change simultaneously. To keep the work straightforward, the flow rates were kept at constants (of 16 ml/min and 4 ml/min for water and precursor, respectively) in studying the effect of crystallization temperature and time (will be discussed in the upcoming sections). In future studies, a more detailed consideration of reactor parameters including reactor diameter, flow rates, temperatures, fluid properties, mixing regimes, etc. should be considered when optimizing the process

3.5 Effect of Reaction Temperature on Conversion

The kinetics of zeolite crystallization are strongly temperature dependent. Crystal grows faster at higher temperatures, because increasing the temperature accelerates the dissolution and diffusivity of nutrient species that facilitates supersaturation [69], which is the driving force for nucleation and crystal growth in liquid solutions [27]. In continuous flow hydrothermal reactor, the instantaneous heating of the zeolite precursor to a very high temperature creates a high degree of supersaturation that significantly accelerates crystallization. Nevertheless, an optimum crystallization temperature exists depending on the procedure. Overly high temperature can have adverse effects on crystallization, including a decrease in crystallinity [70], enhanced decomposition of OSDA to cause slower crystallization rate [59], and the formation of a dense phase or zeolite counterparts. Selecting an optimum temperature is hence important to achieve the most crystalline product.

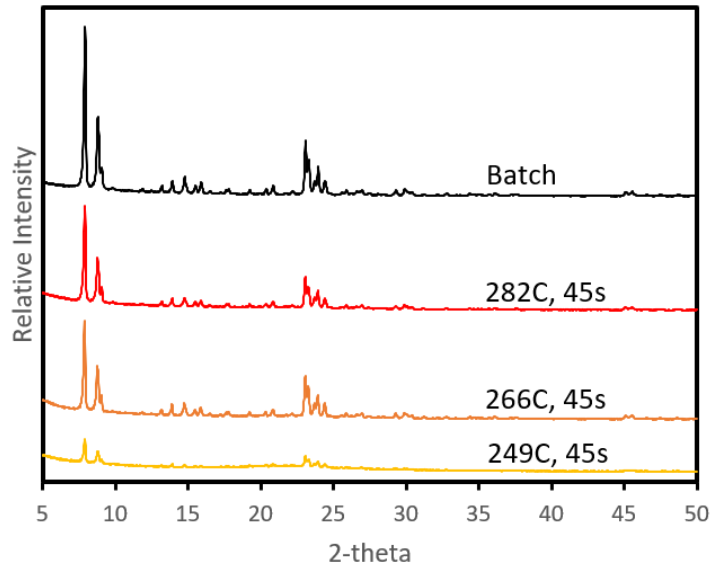


Figure 19. XRD patterns of products obtained in continuous flow synthesis in a 1/2 "tubular reactor at different temperatures in 45 s. The feed conditions were precursor at 4 ml/min, 25 C, water at 16 ml/min.

Fig.19 shows the XRD patterns of the products obtained from the continuous flow reactor at different temperatures after 45s. It is shown that the crystallinity of the synthesized samples increases with increasing the temperature from 249 °C to 266 °C, while the XRD patterns of 266 °C and 282 °C have similar peak intensities, suggesting that synthesis at 282 °C did not further prompt a higher degree of crystallinity. SEM images (Fig.20) were taken to investigate the conversion of the samples. It was observed that the sample synthesized at 266 C was greatly improved in crystallization over the sample synthesized at 249 C, indicated by an increase in the crystal fraction and a decrease in the amount/size of the unconverted precursor particles. In contrast, the product synthesized at 282 °C did not show an as significant improvement in conversion. The samples obtained at 266 °C and 282 °C both contain a fair amount of unconverted precursor particles, and the volume fraction of ZSM-5 crystals within the two samples are also similar. This explains why the two samples showed similar peak intensities by XRD, since the intensity of an XRD pattern is directly proportional to the volume fraction of the components or phases producing it [71]. Even though no apparent improvement in conversion was observed at 282 °C, the zoomed-in SEM images did reveal that the crystals formed at 282 °C are more grown compared to those formed 266 °C as the crystals formed at 282 °C are larger in size and sharper in edges. Both the XRD and SEM results indicate that the rate of crystal growth is slowed down at 282 °C.

One possible explanation for the observation is that the crystallization rate slowed down at 282 °C due to the faster decomposition of OSDA at higher temperatures. Liu et al. reported adverse temperature effects in their study on the synthesis of ZSM-5 zeolite at different temperatures between 240 °C to 300 °C [59]. They observed that the crystallization rate became slower at temperatures higher than 260 °C. The synthesis at 300 C only prompted a faster

crystallization rate with a very short synthesis period, and the rate was not sustained in the latter stage of the synthesis. One probable explanation for the observation is the low stability of OSDA at elevated temperatures. At higher temperatures, OSDA decomposition happened faster, because of which the crystal growth rate is slower in the later stages of the synthesis. It is likely that the synthesis at 282 °C underwent a worse degree of OSDA decomposition that slowed down the rate of crystallization. Therefore, the sample crystallinity was not significantly improved compared to 266 °C.

The crystallization rate can be greatly accelerated by increasing the crystallization temperature, but it should be noted that there is also an optimum temperature and increasing beyond this optimum point can lead to adverse temperature effects, including a slower crystallization rate. Crystallization was observed to slow down at 282 °C, and it is likely caused by the enhanced decomposition of OSDA at a higher temperature. The results indicate that improving the crystallization temperature beyond 282 °C will not further prompt product crystallinity. Thus, improving the residence time is needed to reach target crystallinity.

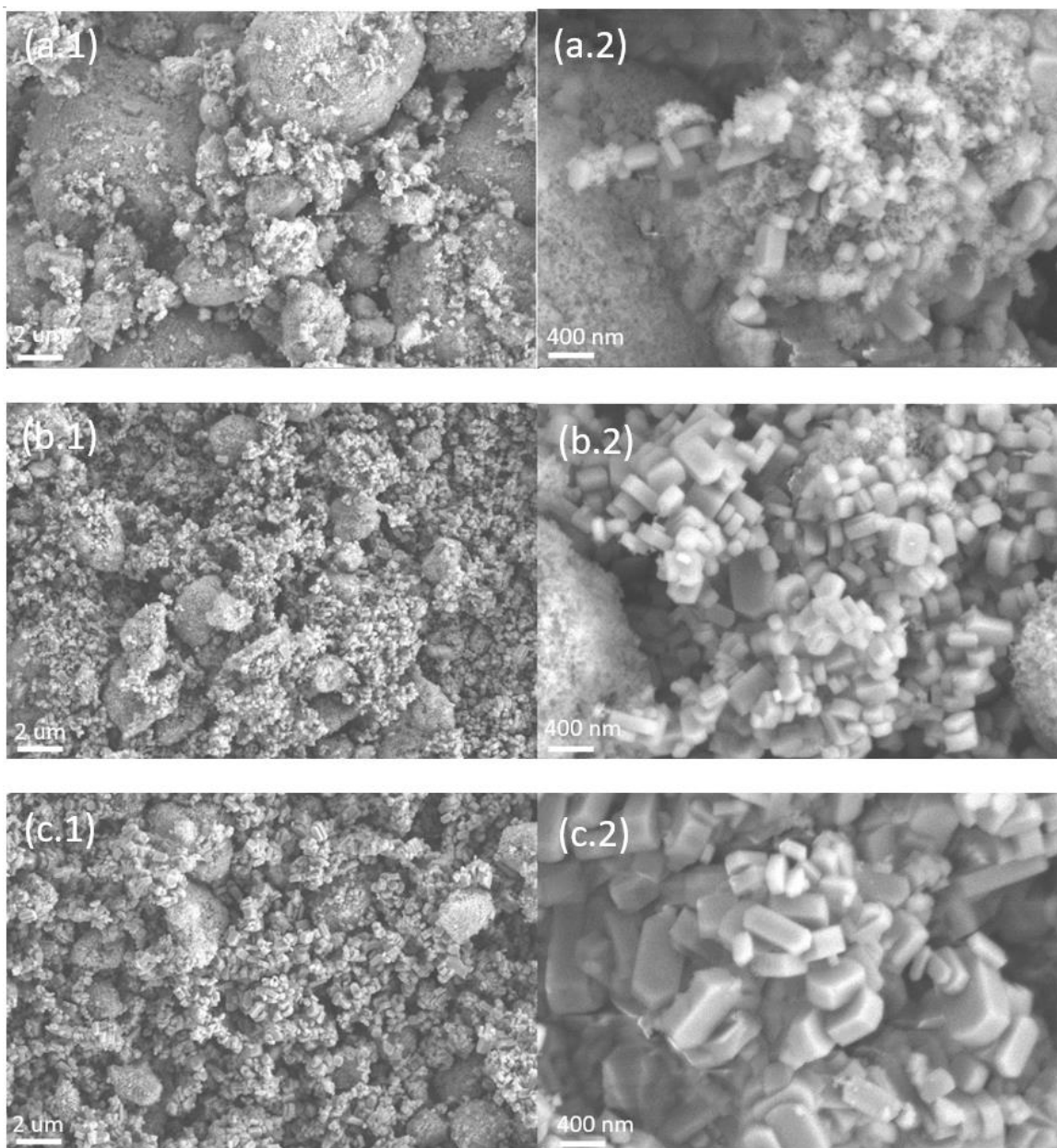


Figure 20. SEM images of samples obtained from the continuous flow reactor ½'' (a) at 249 °C, 45 s, (b) 266 °C, 45s, (c) 282 °C, 45s, at different magnifications (left) 5 k and (right) 25 k.

3.6 Effect of Residence time on Crystallinity and Particle Size

Crystallization time is an important factor for zeolite synthesis. A handful of studies done in batch synthesis have shown that crystallinity and crystal size increase with crystallization time. As discussed in the last section, increasing the temperature did not further prompt crystallinity; residence time is hence increased to achieve a higher product crystallinity.

The reactor length was adjusted to achieve different residence times whilst the flow rates were kept the same. Fig. 21a shows the XRD patterns of the products obtained from the continuous flow reactor after 45s, 60s and 75s, and the peaks are zoomed-in at between 22-25 for a clear comparison (Fig.21b). It can be observed that the product crystallinity increases along with increasing the residence time. After a synthesis time of 75 s, a product with a comparable crystallinity (ca. 95%) to batch-synthesized ZSM-5 was obtained. Compared to the batch ZSM-5 XRD patterns, the 75 s XRD peaks centered at about 23.15 ° appear to be slightly right-shifted, and the proportion of the doublets is smaller. Peak deconvolution (Fig.S5) shows the shift is a result of peak broadening, indicating that the crystallographic phases (501) generating the peaks at 23.15° are less crystalline. SEM images of the products are shown in Fig.22. The particle size remains approximately constant in the samples obtained in 60 s and 75 s. This is because, at high enough temperatures, crystal growth can reach equilibrium in a short period of time so that the effect of crystallization time on particle size is reduced over time [70]. In continuous flow synthesis, the direct mixing generates a high temperature at which the dissolution of nutrients happens at such a fast rate that it pushes the solution to a high degree of supersaturation that causes a burst nucleation step in the initial stage of the synthesis, generating a large number of small nuclei. The nucleation threshold is quickly passed as the burst nucleation quickly brings the nutrient concentration back below the critical nucleation threshold [30, 45]. As the burst

nucleation generates a large number of small nuclei, nutrients in the solution are quickly consumed than if it was at a lower temperature when crystals continue to grow larger as nutrient species keep dissolving at a slower rate over time. Therefore, the particles obtained in a rapidly achieved high-temperature condition may primarily be those from the nuclei generated in the initial phase of the reaction.

The SAR of the product synthesized in 75 seconds using the continuous flow reactor is 111, which is comparable to the batch-synthesized product with a SAR of 119. BET surface area of the continuous product was 337.6 cm² /g, which is also comparable to the batch synthesized product with a BET surface area of 337.0 cm² /g.

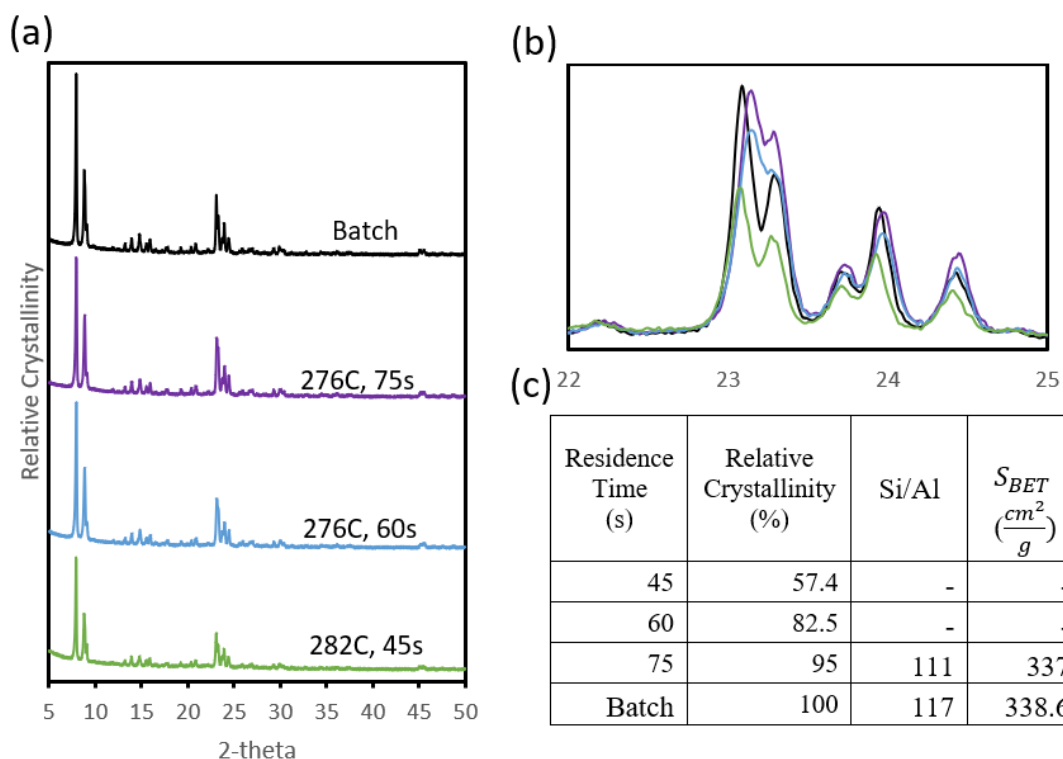


Figure 21. (a) XRD patterns of products obtained in continuous flow synthesis in a 1/2 "tubular reactor at ~280 °C in different residence times. The feed conditions were precursor at 4 ml/min, 25 C, water at 16 ml/min. (b) Zoomed-in XRD patterns of the products between 22-25. (c) Relative crystallinity of the products obtained in the different residence times as well as the silicon to aluminum ratio and the BET surface area of the 75 s and batch synthesized samples.

However, the particles synthesized after 45 s appear to have distinct shape/size compared to those synthesized in 60 s and 75 s. One may first notice that the 45s synthesis was done at a slightly higher temperature, but the temperature is not likely the determinant here because the products obtained at various temperatures presented in the previous section also yielded cubic or coffin-shaped crystals. Such an observation can neither be ascribed to the differences in residence time because there is no driving force for large crystals to dissolve back into the solution to form into smaller crystals that are less stable. A possibility for this observation is that

the mixing condition differed in the synthesis at 45 s, because the temperature of water, whose properties depend on temperature, in the 45 s synthesis was slightly higher (less than 10 °C) than in the other two synthesis (reflected in the higher reactor temperature of 282 °C). The change in density and viscosity of water between the 45 s synthesis and the other two synthesis might result in variations in the mixing regime. Studies on CHFS of metal nanoparticles show that the size and shape of the final products are heavily influenced by the supercritical water and metal salt solution mixing behavior [61, 67, 68]. Further investigations are necessary to understand the effect of mixing behavior on the shape and size of ZSM-5 particles formed. In fact, it is more likely that multiple factors simultaneously impact the size and the shape of crystals. In the future, systematic studies are necessary to understand the correlations between particle morphology/size and different synthesis conditions (temperature, flow rates, flow properties, PH, precursor formula, etc.) to achieve a highly controlled synthesis.

By increasing the residence time, highly crystalline ZSM-5 particles were successfully synthesized from the continuous flow reactor. Synthesis at 276 C after 75 s yielded ZSM-5 zeolites with comparable crystallinity to batch synthesized products. As expected, crystallinity in a continuous flow reactor increases with increasing the residence time. Different than batch synthesis, no apparent increase in particle size was observed at a longer residence time because the effect of crystallization time on particle size at higher temperatures is minimized.

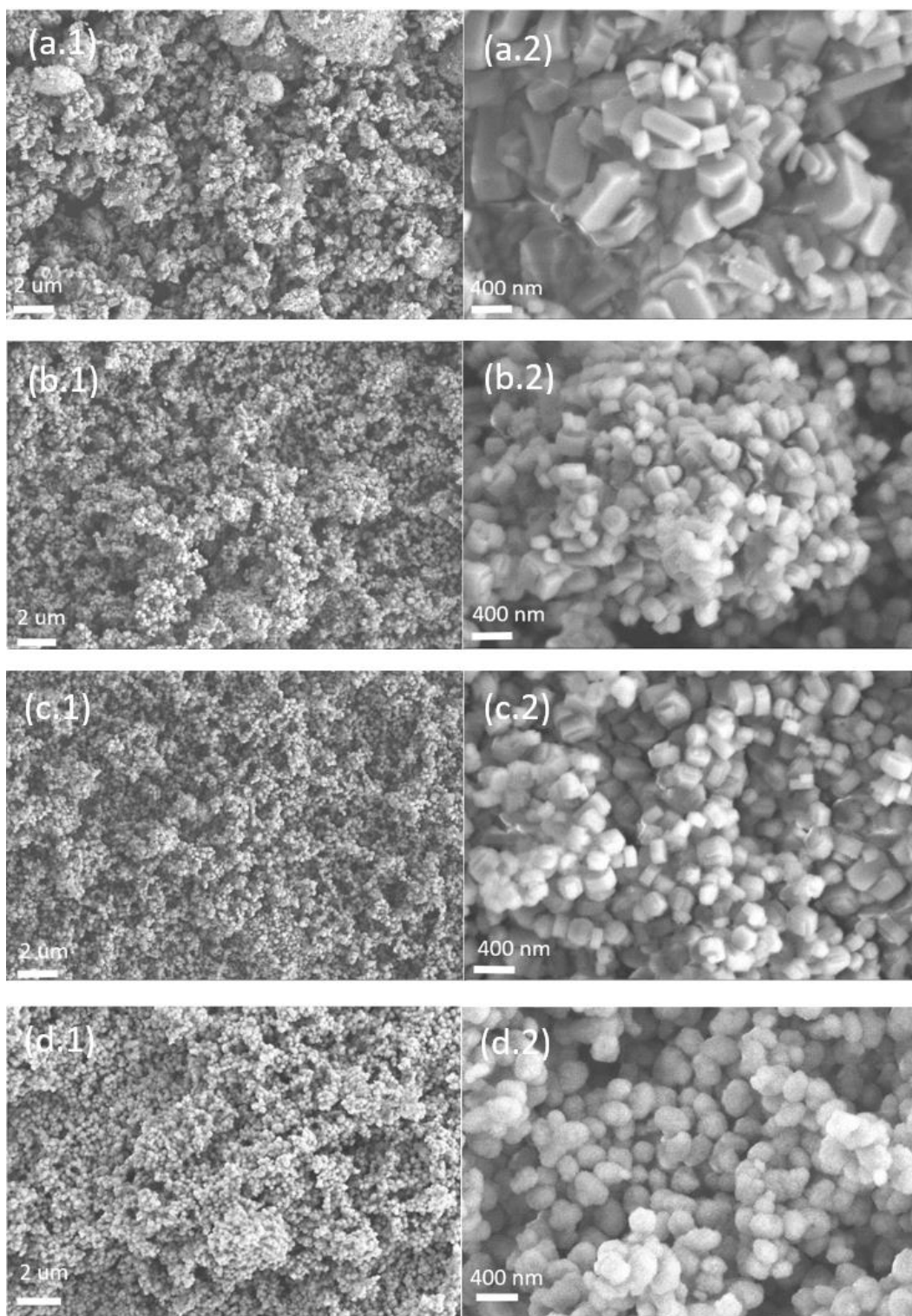


Figure 22. SEM images of the samples obtained from the continuous flow reactor $\frac{1}{2}$ " (a) at 282 °C, 45 s, (b) 276 °C, 60s, (c) 276 °C, 75 s, (d) batch synthesis at 170 °C, 24 hr., at different magnifications (left) 5 k and (right) 25 k.

3.7 Continuous vs Batch Synthesis – Yield and Production Rate

Sedimentation and fouling of solid particles have led to a much-decreased yield of zeolite in the continuous flow system. The yield of zeolite is calculated as the following:

$$\text{Yield of Zeolite} = \frac{\text{weight of calcined product}}{\text{weight of Al}_2\text{O}_3 \text{ and SiO}_2 \text{ in the initial precursor gel}} \quad (3-1)$$

Fig.23 shows the pressure and temperature profile of the system during a typical continuous operation (at 270 C, 75s). To achieve continuous operation, a set of parallel filters and a backflush pump were installed as shown in Fig S3. During the operation, the product flow was allowed to pass through filter 1. When filter 1 started to clog and the upstream pressure reached 105 bar, the three-way valves (3V-1 and 3V-2) were switched to direct the flow into a clean filter 2, allowing the operation to proceed further. At the same time, a backflush pump was used to clean the deposited particles out of filter 1. As the upstream pressure again reached 105 bar, it was then switched back to filter 1 while the second filter was being flushed to allow a continuous operation. One can see that the system pressure increased at a slower rate in the first 10 mins of the operation, indicating that there was a slow buildup of solid particles in the system until the product stream reached a high concentration of solids to cause rapid blockages in the filters.

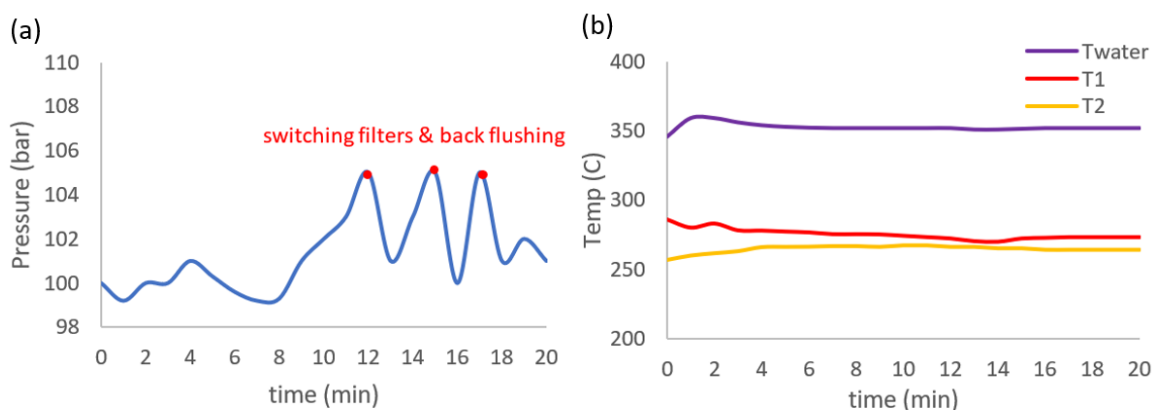


Figure 23. (a) Pressure profile and (b) temperature profile during continuous synthesis in a 1/2'' reactor at 276 C, 75s.

Particles were collected from four different ends (Fig.S6), 1) aqueous slurry collected at the reactor outlet during the operation, 2) aqueous slurry flushed out of the filters during the operation, 3) particles deposited onto the filters that were retrieved after the taking out the filters, 4) residual particles cleaned out from the system (from the mixing element to the filters) after opening the system. As can be seen from the SEM images and particle size distributions (Fig.24), the particles collected from the reactor outlet, the backflush outlet, and the filters have similar sizes and morphology, while the residual particles cleaned out from the system show larger particles sizes primarily due to a long time they spent in the reactor (at high T and high P). In addition, the shapes of residual particles are less homogeneous as compared to the outlet particles, which could be caused by poorly defined growth conditions in the system. The sample crystallinities (determined from XRD) were consistent (95% and 97%) for the outlet and the backflush, respectively. Therefore, products could be collected from both the reactor and backflush outlets, while the particles that were stuck in the system, which were collected after disassembling the system, were not taken as the product because they spent much longer times in system under poorly defined conditions.

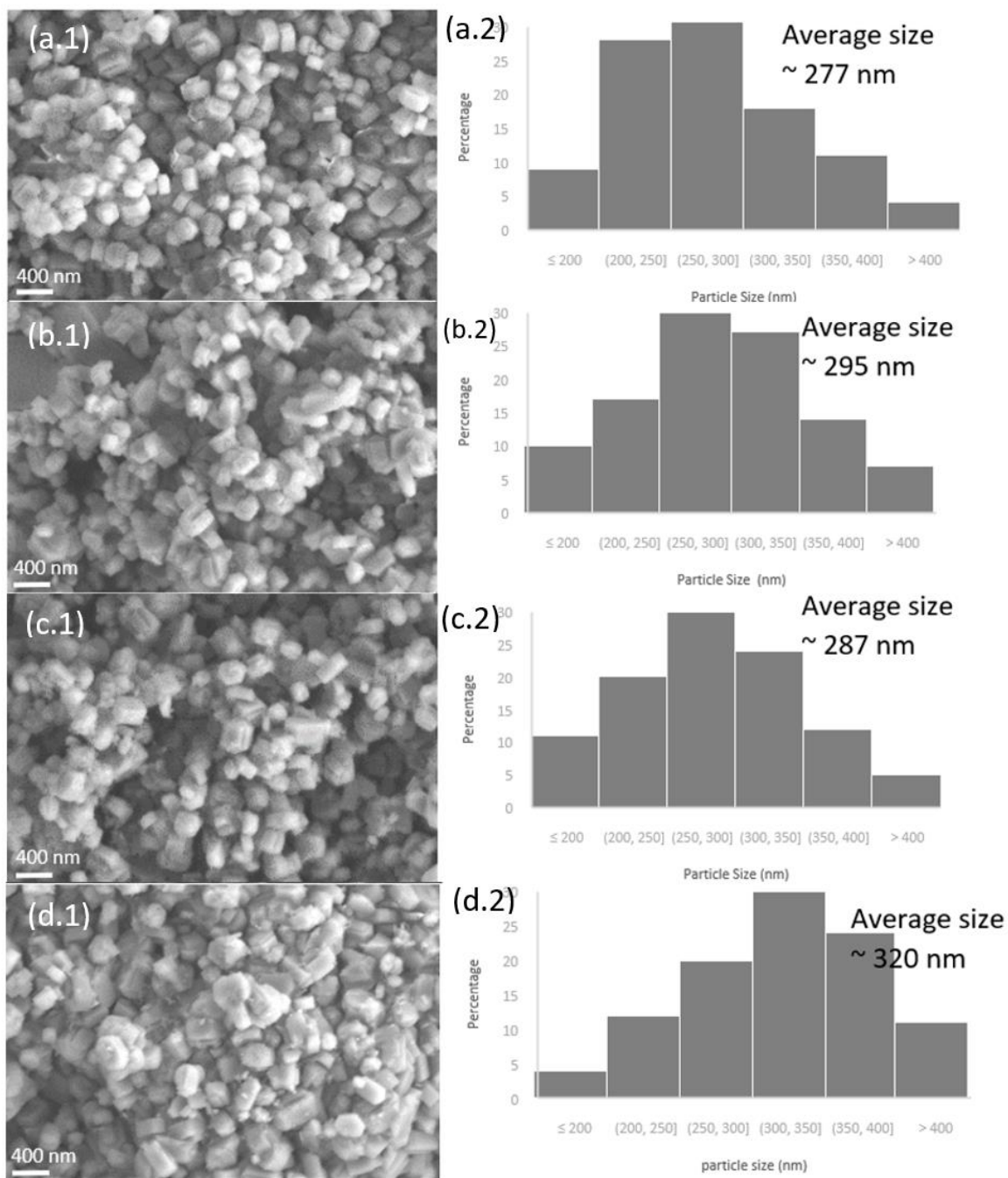


Figure 24. SEM images (left) and particle size distributions (right) of samples collected (a) at the outlet, (b) from solids flushed out of the filters (c) from the solids stuck in the filters, (d) residual particles cleaned out of the system.

Table.1 shows the mass of the particles (after calcination) collected from each of the sources. Only half (50.4 wt.%) of all the solids formed were being able to be collected (at the outlet and from the backflush) during the operation, while the other half of the particles (49.6 wt.%) was stuck in the system due to three reasons: 1) zeolite particles attached to the wall in the hot reactor zone (Fig.25a), 2) deposition of zeolite particles in the filters (Fig.25b), and 3) sedimentation of zeolite particles to the bottom of tubing in the downstream reactor where the system was not effectively being vibrated (fig.25c).

Table 1. Weight of samples collected from different sources

	Weight (g)	Weight %	Yield %
1) Outlet	3.43	21.2	12.7
2) Back Flush	4.72	29.2	17.5
3) Filter	1.06	6.6	3.9
4) Residue	6.97	43.1	25.8
Total	16.18	100.0	59.8

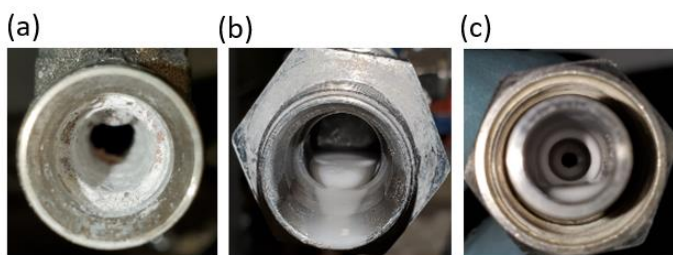


Figure 25: Photos showing (a) reactor fouling, (b) particle deposition in the filter, (c) particles settled to the bottom of tubing

Assuming a continuous operation, the production rate of ZSM-5 in the continuous flow reactor is 0.41 g ZSM-5/min, which equals to ~ 590 g ZSM-5/day. With all six hydrothermal reactors (45 ml each) existing in the lab running in parallel, the production rate is ~ 55 g ZSM-5/day. The volume of the continuous reactor is about 33 ml, which generated a much higher time-space yield of ~ $751 \frac{kg}{m^3h}$, compared to that of the autoclave batch synthesis which is ~ $8.5 \frac{kg}{m^3h}$. Even as half of the solids were stuck in the system, the production rate in the continuous flow reactor is still several times higher than that of batch synthesis. Nevertheless, the process definitely needs optimization. An immediate improvement can be made is to add a second air-driven vibrator to the downstream reactor to reduce the particle sedimentation in the tubing. As discussed in section 1.1.5, many research groups have demonstrated the use of specially designed reactor components to prevent or reduce particle attachment and aggregation in flow systems. For future studies, designing and engineering reactor components that are suitable for a high solid forming synthesis will be critical steps towards scale-up of the process.

4.0 Conclusions and Outlooks

4.1 Conclusion

This thesis demonstrates the continuous synthesis of highly crystalline ZSM-5 zeolite with a vastly accelerated synthesis time and a high production rate of > 590 g/day. The continuous synthesis set up developed in this project can operate with much higher production efficiency comparing with batch synthesis, demonstrating its large potential for scale-up synthesis of ZSM-5. The approach is based on the direct mixing of the zeolite precursor with pressurized hot water in a continuous flow reactor, where high temperatures can be immediately reached to accelerate ZSM-5 crystallization, then followed by rapid quenching of the product stream to prevent undesired reactions. Although a high temperature greatly accelerates zeolite crystallization, an optimum temperature exists and increasing beyond this temperature will not further prompt crystallization. As expected, crystallinity increases with increasing the residence time. The idea of ‘the directing mixing’ is a fairly simple concept, but in practice, the successful implementation of a continuous process, especially in the presence of high solid contents, can be quite complex, with a number of hurdles to overcome. Key issues identified in developing the flow reactor have been discussed, including particle attachment to reactor surfaces, undesired preheating of precursor feed, and solid particle deposition in the filters protecting the back pressure regulator, which led to ill-defined conditions and blockages. The approaches taken to address these problems in this study were limited to what is available to us. To move towards scaling up and commercialization of this process, designing and engineering reactor components

suitable for a high solid forming flow synthesis will be critical for a stable and controlled operation.

4.2 Outlook

Building upon this thesis, and with respect to the lack of studies on continuous flow hydrothermal synthesis of zeolites, the following topics are worth investigating:

- Improving the design and engineering of reactor components

The laboratory-scale flow reactor developed in this work can only serve as a ‘proof of concept’ that highly crystalline ZSM-5 can be achieved within tens of seconds using the directing mixing approach, and there are many optimizations needed. The components used to build up this system are only limited to what is available to us. For example, using a standard off-the-shelf T-piece mixer is convenient, but it does not offer a uniform mixing. In future works, a full consideration (flow rates, temperature, heat exchange and buoyancy/momentum between the mixing streams, etc.) should be put into designing and engineering a customized mixing element for this process via CFD modeling and experimentations. Minimizing the accumulation of solid particles in different components (reactor, filters, tubing) of the system will be the key step towards scaling-up of this process. As introduced in section 1.1.5, a handful of studies have come up with specially designed reactor components to address fouling and blockage issues. Designing and engineering reactor components suitable for a high solid forming synthesis will be critical for a stable and continuous operation.

- Working towards a controlled synthesis of ZSM-5

The morphology and size of zeolite particles are important factors contributing to their properties and applications. So far, we lack understanding and control over the morphology/size of ZSM-5 particles synthesized in the continuous flow reactor. Studies on CFHS of metal nanoparticles have shown that the size and morphology of products can be controlled by manipulating the synthesis conditions such as PH, temperature, flow rate, etc. The knowledge may be transferable to the CHFS of zeolites. In addition, the mixing profile is conceivably an important factor contributing to the particle morphology/size because nucleation/growth occurs immediately upon the mixing of zeolite precursor and pressurized hot water and preferred crystallographic orientation for growth largely dependent on the condition upon the mixing. It is not straightforward to alter one variable without changing the others in the continuous flow reactor; therefore, systemic studies are necessary to understand the correlations between particle morphology/size and different synthesis conditions (temperature, flow rates, flow properties, PH, precursor formula, etc.) to achieve highly controlled synthesis in the future.

- Well-tuning the zeolite precursor

The current precursor recipe and aging conditions adopted from previous work have a high solid content. Large particles settled out of the precursor gel in just a few minutes upon standing. During continuous synthesis, phase separation of precursor gel happens over time in the syringe pump, leading to an inaccurate feed concentration. The large particles also damage the pump seals and result in pump leakage. A pump seal usually wears out after only two or three

syntheses. Tuning the precursor formula and the aging conditions to reduce the precipitation of solid particles will be critical to address these problems.

Preliminary tests have indicated that much-diluted precursor (with an equal weight of water) prior to the synthesis enabled a much more stable operation and delayed filter blockages compared to running the regular precursor. Tuning the precursor formula in an effort to lower the solid content in the product stream is conducive to a smooth operation, albeit with a lower production rate.

- Incorporating transitional metal into ZSM-5 in continuous synthesis

Encapsulating transitional metal nanoclusters in zeolites creates bifunctional catalysts that combine the nanoclusters' excellent catalytic activity with the crystalline microporous materials' great stability and unique shape selectivity. Incorporating metal particles into this continuous production would be highly desirable. Preliminary studies on synthesizing 1wt% and 2wt% Fe-ZSM-5 yielded poorly crystallized particles due to a much slower crystallization rate in the presence of Fe. The addition of Fe in the precursor gel also showed much-increased viscosity of the precursor gel, as well as differences in wall interactions, raising renewed concerns with fouling and blockage of the continuous reactor.

Appendix A Supplemental Materials

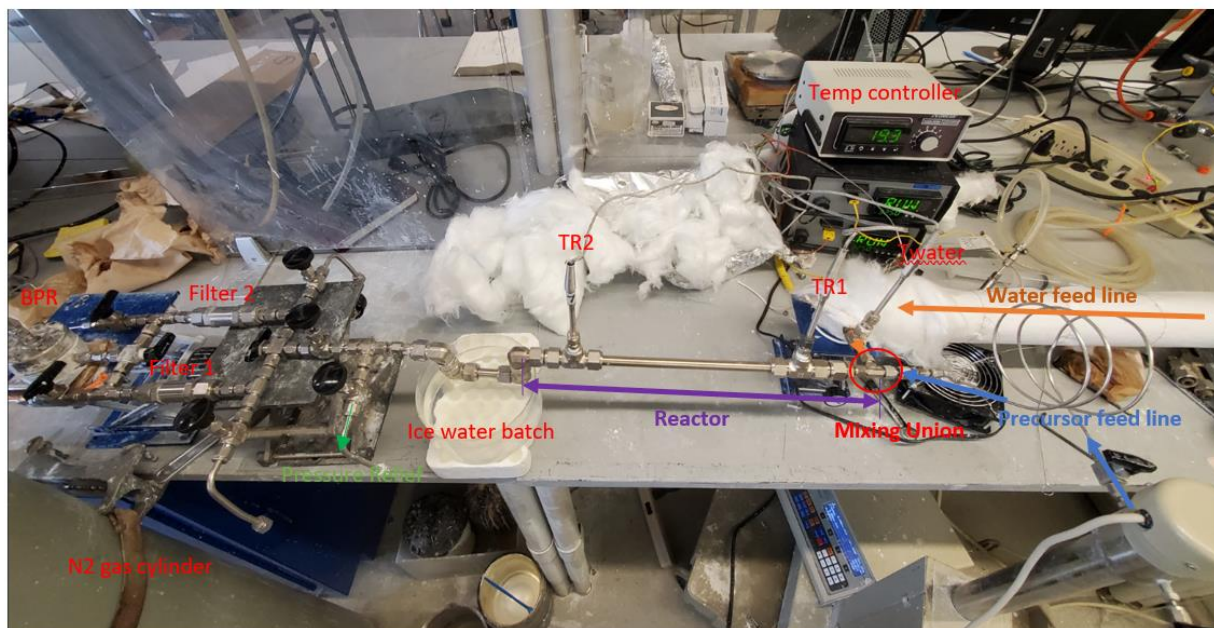


Figure S 1. Detailed illustration of the continuous flow apparatus used for the ultrafast synthesis of zeolites. Please see Fig 27 to Fig 29 for zoomed in views of specific sections.



Figure S 2. Photo showing (a) reactor ready for running synthesis, (b) the reactor after removing the insulations and the vibrator. The reactor length is defined as the distance from the midpoint in the T mixer to the end of the tubular reactor as shown in the picture.

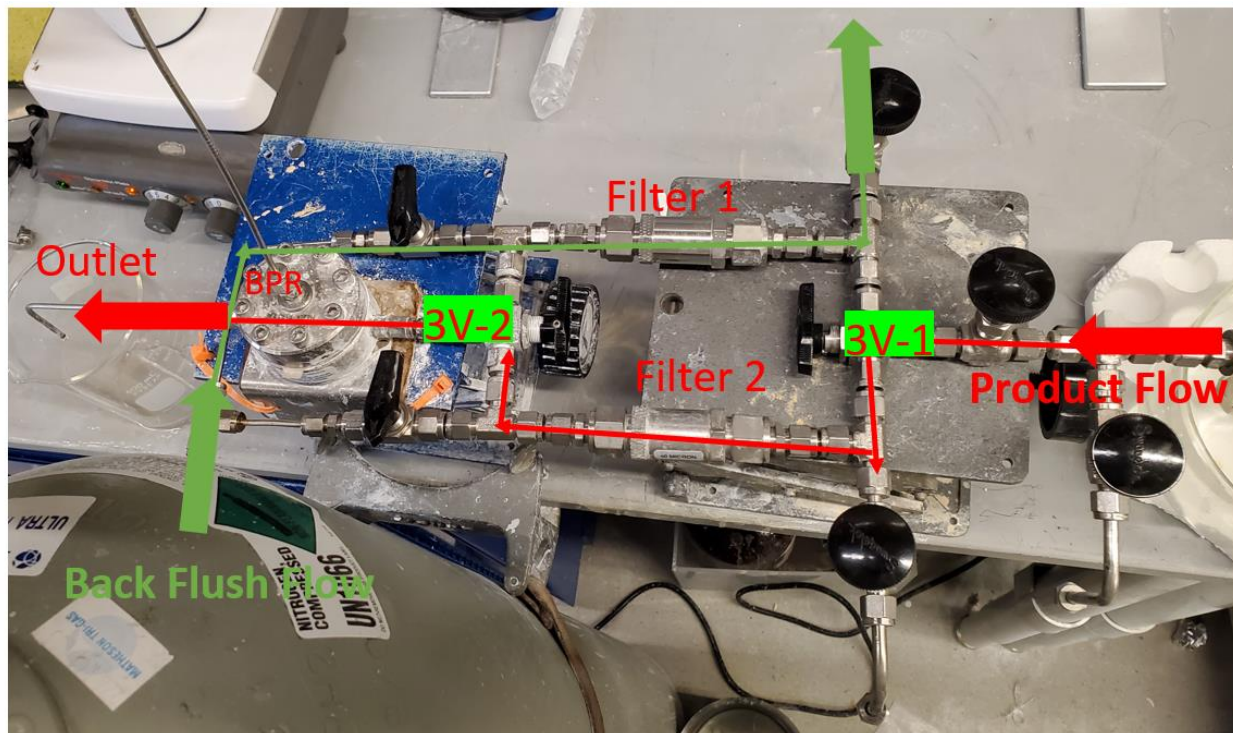


Figure S 3. Detailed illustration of the parallel filter setup. When Filter 1 is blocked, 3V-1 and 3V-2 are switched to Filter 2 to allow a continuous flow of product stream (Red Line) while Filter 1 is being flushed with water (Green line).

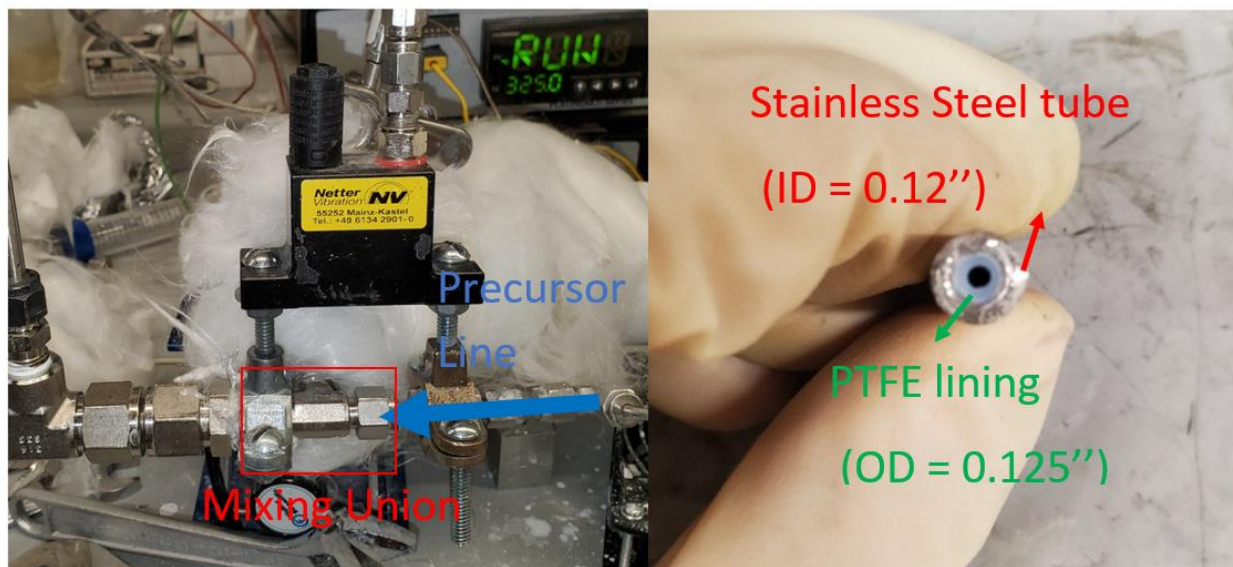


Figure S 4. Photo showing (a) the connection of vibrator to system tubing, (b) PTFE-lined tube in precursor feed line.

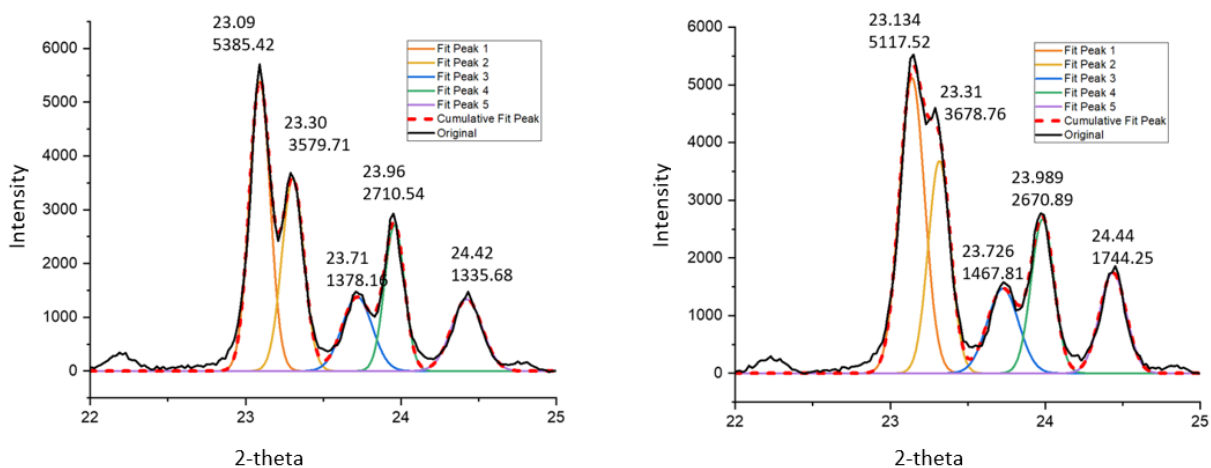


Figure S 5. Peak deconvolution on XRD patterns of (a) batch synthesized ZSM-5, (b) product obtained at 276 °C, 75s in continuous synthesis. The position (2-theta) and height (intensity) of the deconvoluted peaks are shown on the top of each individual peak. It can be observed that the peaks centered at 23.15° in the sample in continuous synthesis are broadened and the ratio of the doublets is smaller

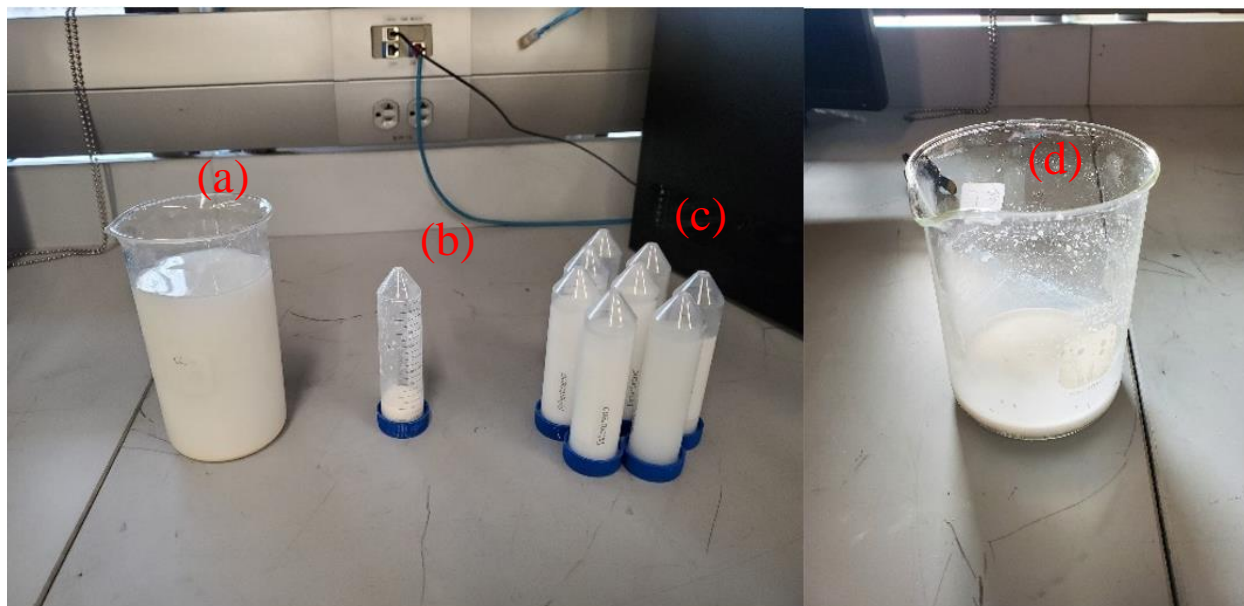


Figure S 6. Samples collected from a typical continuous flow synthesis after 20 mins. (a) Aqueous slurry flushed out of the filters, (b) deposited particles retrieved from the filters, (c) aqueous slurry collected and the outlet, (d) residue cleaned out of the system.

Bibliography

1. Moshoeshe, M., M.S. Nadiye-Tabbiruka, and V. Obuseng, *A review of the chemistry, structure, properties and applications of zeolites*. Am. J. Mater. Sci, 2017. **7**(5): p. 196-221.
2. Król, M., *Natural vs. synthetic Zeolites*. 2020, Multidisciplinary Digital Publishing Institute. p. 622.
3. Baerlocher, C., L.B. McCusker, and D.H. Olson, *Atlas of zeolite framework types*. 2007: Elsevier.
4. Barrer, R.M., 33. *Synthesis of a zeolitic mineral with chabazite-like sorptive properties*. Journal of the Chemical Society (Resumed), 1948: p. 127-132.
5. Cundy, C.S. and P.A. Cox, *The hydrothermal synthesis of zeolites: history and development from the earliest days to the present time*. Chemical reviews, 2003. **103**(3): p. 663-702.
6. Argauer, R.J. and G.R. Landolt, *Crystalline zeolite ZSM-5 and method of preparing the same*. 1972, Google Patents.
7. Kokotailo, G., et al., *Structure of synthetic zeolite ZSM-5*. Nature, 1978. **272**(5652): p. 437-438.
8. Kubů, M., R. Millini, and N. Žilková, *10-ring Zeolites: Synthesis, characterization and catalytic applications*. Catalysis Today, 2019. **324**: p. 3-14.
9. Egeblad, K., et al., *Templating mesoporous zeolites*. Chemistry of Materials, 2008. **20**(3): p. 946-960.
10. Mgbemere, H., I. Ekpe, and G. Lawal, *Zeolite synthesis, characterization and application areas: a review*. 2017.
11. Dyer, A., *An introduction to zeolite molecular sieves*. 1988.
12. Bleken, F., et al., *Conversion of methanol over 10-ring zeolites with differing volumes at channel intersections: comparison of TNU-9, IM-5, ZSM-11 and ZSM-5*. Physical Chemistry Chemical Physics, 2011. **13**(7): p. 2539-2549.
13. Yilmaz, B. and U. Müller, *Catalytic applications of zeolites in chemical industry*. Topics in Catalysis, 2009. **52**(6): p. 888-895.
14. Lunevich, L., *Aqueous silica and silica polymerisation*. Desalination-Challenges and Opportunities, 2019. **6**: p. 1-19.

15. Van Grieken, R., et al., *Anomalous crystallization mechanism in the synthesis of nanocrystalline ZSM-5*. *Microporous and Mesoporous Materials*, 2000. **39**(1-2): p. 135-147.
16. Katović, A., et al., *Role of gel aging in zeolite crystallization*. 1989.
17. Czarna-Juszkiewicz, D., J. Cader, and M. Wdowin, *From coal ashes to solid sorbents for hydrogen storage*. *Journal of Cleaner Production*, 2020. **270**: p. 122355.
18. Cundy, C.S. and P.A. Cox, *The hydrothermal synthesis of zeolites: Precursors, intermediates and reaction mechanism*. *Microporous and mesoporous materials*, 2005. **82**(1-2): p. 1-78.
19. Davis, M., *Molecular sieves: Principles of synthesis and identification: By R. Szostak*. Van Nostrand-Reinhold, New York, 1988. \$69.95. 1989, Academic Press.
20. Flanigen, E., *Molecular sieves-Advances in Chemistry, Chapter 10 A Review and New Perspectives in Zeolite Crystallization*. 1973, American Chemical Society.
21. Grand, J., H. Awala, and S. Mintova, *Mechanism of zeolites crystal growth: new findings and open questions*. *CrystEngComm*, 2016. **18**(5): p. 650-664.
22. Itabashi, K., et al., *A working hypothesis for broadening framework types of zeolites in seed-assisted synthesis without organic structure-directing agent*. *Journal of the American Chemical Society*, 2012. **134**(28): p. 11542-11549.
23. Kamimura, Y., et al., *Critical factors in the seed - assisted synthesis of zeolite beta and “green beta” from OSDA - free Na⁺ - aluminosilicate gels*. *Chemistry—An Asian Journal*, 2010. **5**(10): p. 2182-2191.
24. Miyake, K., et al., *Solvent - and OSDA - Free Synthesis of ZSM - 5 Assisted by Mechanochemical and Vapor Treatments*. *ChemistrySelect*, 2017. **2**(25): p. 7651-7653.
25. Kamimura, Y., et al., *OSDA-free synthesis of MTW-type zeolite from sodium aluminosilicate gels with zeolite beta seeds*. *Microporous and mesoporous materials*, 2012. **163**: p. 282-290.
26. Jain, R. and J.D. Rimer, *Seed-Assisted zeolite synthesis: The impact of seeding conditions and interzeolite transformations on crystal structure and morphology*. *Microporous and Mesoporous Materials*, 2020. **300**: p. 110174.
27. Kashchiev, D. and G. Van Rosmalen, *Nucleation in solutions revisited*. *Crystal Research and Technology: Journal of Experimental and Industrial Crystallography*, 2003. **38**(7 - 8): p. 555-574.
28. LaMer, V.K. and R.H. Dinegar, *Theory, production and mechanism of formation of monodispersed hydrosols*. *Journal of the american chemical society*, 1950. **72**(11): p. 4847-4854.

29. Arshadi, S., J. Moghaddam, and M. Eskandarian, *LaMer diagram approach to study the nucleation and growth of Cu₂O nanoparticles using supersaturation theory*. Korean Journal of Chemical Engineering, 2014. **31**(11): p. 2020-2026.
30. Dunne, P.W., et al., *Continuous-flow hydrothermal synthesis for the production of inorganic nanomaterials*. Philosophical Transactions of the Royal Society A: Mathematical, Physical and Engineering Sciences, 2015. **373**(2057): p. 20150015.
31. Cejka, J., *Introduction to zeolite science and practice*. 2007: Elsevier.
32. Shevlin, S., *Looking deeper into zeolites*. Nature Materials, 2020. **19**(10): p. 1038-1039.
33. Yamada, H., et al., *Structural Evolution of Amorphous Precursors toward Crystalline Zeolites Visualized by an in Situ X-ray Pair Distribution Function Approach*. The Journal of Physical Chemistry C, 2019. **123**(46): p. 28419-28426.
34. Burkett, S.L., *Mechanisms of structure direction in zeolite synthesis*. 1995, California Institute of Technology.
35. Liu, Z., et al., *Ultrafast synthesis of zeolites: breakthrough, progress and perspective*. Inorganic Chemistry Frontiers, 2019. **6**(1): p. 14-31.
36. Meng, X. and F.-S. Xiao, *Green routes for synthesis of zeolites*. Chemical reviews, 2014. **114**(2): p. 1521-1543.
37. Robson, H., *Verified synthesis of zeolitic materials*. 2001: Gulf Professional Publishing.
38. Wu, Q., et al., *110th anniversary: sustainable synthesis of zeolites: from fundamental research to industrial production*. Industrial & Engineering Chemistry Research, 2019. **58**(27): p. 11653-11658.
39. Burcham, C.L., A.J. Florence, and M.D. Johnson, *Continuous manufacturing in pharmaceutical process development and manufacturing*. Annual review of chemical and biomolecular engineering, 2018. **9**: p. 253-281.
40. Baumann, M., et al., *A perspective on continuous flow chemistry in the pharmaceutical industry*. Organic Process Research & Development, 2020. **24**(10): p. 1802-1813.
41. Porta, R., M. Benaglia, and A. Puglisi, *Flow chemistry: recent developments in the synthesis of pharmaceutical products*. Organic Process Research & Development, 2016. **20**(1): p. 2-25.
42. Kortshagen, U.R., et al., *Nonthermal plasma synthesis of nanocrystals: fundamental principles, materials, and applications*. Chemical reviews, 2016. **116**(18): p. 11061-11127.

43. Arutanti, O., et al., *Tailored synthesis of macroporous Pt/WO₃ photocatalyst with nanoaggregates via flame assisted spray pyrolysis*. *AIChE Journal*, 2016. **62**(11): p. 3864-3873.
44. Aksomaityte, G., M. Poliakoff, and E. Lester, *The production and formulation of silver nanoparticles using continuous hydrothermal synthesis*. *Chemical engineering science*, 2013. **85**: p. 2-10.
45. Darr, J.A., et al., *Continuous hydrothermal synthesis of inorganic nanoparticles: applications and future directions*. *Chemical reviews*, 2017. **117**(17): p. 11125-11238.
46. Adschiri, T., K. Kanazawa, and K. Arai, *Rapid and continuous hydrothermal crystallization of metal oxide particles in supercritical water*. *Journal of the American Ceramic Society*, 1992. **75**(4): p. 1019-1022.
47. Gimeno-Fabra, M., et al., *Instant MOFs: continuous synthesis of metal-organic frameworks by rapid solvent mixing*. *Chemical Communications*, 2012. **48**(86): p. 10642-10644.
48. d'Arras, L., et al., *Fast and continuous processing of a new sub-micronic lanthanide-based metal-organic framework*. *New Journal of Chemistry*, 2014. **38**(4): p. 1477-1483.
49. Bayliss, P.A., et al., *Synthesis of metal-organic frameworks by continuous flow*. *Green Chemistry*, 2014. **16**(8): p. 3796-3802.
50. Clark, I., et al., *Towards the Continuous Hydrothermal Synthesis of ZnO@ Mg₂Al-CO₃ Core-Shell Composite Nanomaterials*. *Nanomaterials*, 2020. **10**(10): p. 2052.
51. Ju, J., et al., *Continuous synthesis of zeolite NaA in a microchannel reactor*. *Chemical Engineering Journal*, 2006. **116**(2): p. 115-121.
52. Bonaccorsi, L. and E. Proverbio, *Influence of process parameters in microwave continuous synthesis of zeolite LTA*. *Microporous and mesoporous materials*, 2008. **112**(1-3): p. 481-493.
53. Liu, Z., et al., *Ultrafast synthesis of silicalite-1 using a tubular reactor with a feature of rapid heating*. *Microporous and Mesoporous Materials*, 2016. **223**: p. 140-144.
54. Liu, Z., et al., *Continuous flow synthesis of ordered porous materials: from zeolites to metal-organic frameworks and mesoporous silica*. *Reaction Chemistry & Engineering*, 2019. **4**(10): p. 1699-1720.
55. Aguado, S., et al., *Continuous synthesis of NaA zeolite membranes*. *Microporous and Mesoporous Materials*, 2009. **120**(1-2): p. 170-176.
56. Liu, Z., et al., *Widening Synthesis Bottlenecks: Realization of Ultrafast and Continuous - Flow Synthesis of High - Silica Zeolite SSZ - 13 for NO_x Removal*. *Angewandte Chemie*, 2015. **127**(19): p. 5775-5779.

57. Cundy, C. and J. Zhao, *Remarkable synergy between microwave heating and the addition of seed crystals in zeolite synthesis—a suggestion verified*. *Chemical Communications*, 1998(14): p. 1465-1466.
58. Park, S.-E., et al., *Supramolecular interactions and morphology control in microwave synthesis of nanoporous materials*. *Catalysis surveys from Asia*, 2004. **8**(2): p. 91-110.
59. Liu, Z., et al., *Continuous flow synthesis of ZSM-5 zeolite on the order of seconds*. *Proceedings of the National Academy of Sciences*, 2016. **113**(50): p. 14267-14271.
60. Baber, R., et al., *Synthesis of silver nanoparticles using a microfluidic impinging jet reactor*. *Journal of Flow Chemistry*, 2016. **6**(3): p. 268-278.
61. Gkogkos, G., et al., *Fouling-proof triple stream 3D flow focusing based reactor: Design and demonstration for iron oxide nanoparticle co-precipitation synthesis*. *Chemical Engineering Science*, 2022. **251**: p. 117481.
62. Lester, E., et al., *Impact of reactor geometry on continuous hydrothermal synthesis mixing*. *Materials Research Innovations*, 2010. **14**(1): p. 19-26.
63. Lester, E.H. and B.J. Azzopardi, *Counter current mixing reactor*. 2009, Google Patents.
64. Wakashima, Y., et al., *Development of a new swirling micro mixer for continuous hydrothermal synthesis of nano-size particles*. *Journal of Chemical Engineering of Japan*, 2007. **40**(8): p. 622-629.
65. Hong, S.-A., et al., *Continuous synthesis of lithium iron phosphate (LiFePO₄) nanoparticles in supercritical water: Effect of mixing tee*. *The Journal of Supercritical Fluids*, 2013. **73**: p. 70-79.
66. Zhu, J., et al., *Addressing the viscosity challenge: Ultrafast, stable-flow synthesis of zeolites with an emulsion method*. *Reaction Chemistry & Engineering*, 2018. **3**(6): p. 844-848.
67. Deadman, B.J., et al., *Back Pressure Regulation of Slurry - Forming Reactions in Continuous Flow*. *Chemical Engineering & Technology*, 2015. **38**(2): p. 259-264.
68. Takami, S., et al., *In-situ neutron tomography on mixing behavior of supercritical water and room temperature water in a tubular flow reactor*. *Physics Procedia*, 2015. **69**: p. 564-569.
69. Larlus, O. and V.P. Valtchev, *Control of the morphology of all-silica BEA-type zeolite synthesized in basic media*. *Chemistry of materials*, 2005. **17**(4): p. 881-886.
70. Alipour, S.M., R. Halladj, and S. Askari, *Effects of the different synthetic parameters on the crystallinity and crystal size of nanosized ZSM-5 zeolite*. *Reviews in Chemical Engineering*, 2014. **30**(3): p. 289-322.

71. Alexander, L. and H.P. Klug, *Basic aspects of X-ray absorption in quantitative diffraction analysis of powder mixtures*. Analytical Chemistry, 1948. **20**(10): p. 886-889.